Subcellular specificity of cannabinoid effects in striatonigral circuits

Edgar Soria-Gomez, Antonio Pagano Zottola, Yamuna Mariani, Tifany Desprez, Massimo Barresi, Itziar Bonilla-del Río, Carolina Muguruza, Morgane Le Bon-Jego, Francisca Julio-Kalajzić, Robyn Flynn, et al.

HAL Id: hal-03375577

https://hal.archives-ouvertes.fr/hal-03375577

Submitted on 15 Oct 2021

1 SUBCELLULAR SPECIFICITY OF CANNABINOID EFFECTS IN STRIATONIGRAL

2 CIRCUITS

3

4 Edgar Soria-Gomez[1,2,3,4,5,15,16*], Antonio C. Pagano Zottola[1,2,15], Yamuna
5 Mariani[1,2,15], Tifany Desprez[1,2], Massimo Barresi[2,6], Itziar Bonilla-del-Río[3,4],
6 Carolina Muguruza[7], Morgane Le Bon-Jego[2,6], Francisca Julio-Kalajzić[1,2],
7 Robyn Flynn[8,9], Geoffrey Terral[1,2], Ignacio Fernández-Moncada[1,2], Laurie M.
8 Robin[1,2], Jose F. Olivera da Cruz[1,2], Simone Corinti[1,2], Yasmine Ould Amer[10],
9 Julia Goncalves[1,2], Marjorie Varilh[1,2], Astrid Cannich[1,2], Bastien Redon[1,2], Zhe
10 Zhao[1,2], Thierry Lesté-Lasserre[1,2], Peggy Vincent[1,2], Tarson Tolentino-Cortes[11],
11 Arnau Busquets-García[1,2], Nagore Puente[3,4], Jaideep S. Bains[9], Etienne
12 Hebert-Chatelain[10], Gabriel Barreda-Gómez[11], Francis Chaouloff[1,2], Alexander
13 W. Lohman[8,9,12], Luis F. Callado[7,13], Pedro Grandes[3,4,14], Jerome Baufreton[2,6],
14 Giovanni Marsicano[1,2,16,17*], Luigi Bellocchio[1,2,16*]

15
16 [1]INSERM, U1215 NeuroCentre Magendie, Endocannabinoids and
17 Neuroadaptation, Bordeaux, France; [2]University of Bordeaux; [3]Dept. of
18 Neurosciences, Faculty of Medicine and Nursing, University of the Basque
19 Country UPV/EHU, Leioa, Spain; [4]Achucarro Basque Center for Neuroscience,
20 Leioa, Spain; [5]IKERBASQUE, Basque Foundation for Science; [6]IMN-UMR
21 CNRS 5293 Neurodegenerative Diseases Institute, Bordeaux, France; [7]Dept. of
22 Pharmacology, University of the Basque Country UPV/EHU, Leioa, and Centro
23 de Investigación Biomédica en Red de Salud Mental (CIBERSAM), Spain.
24 [8]Department of Cell Biology and Anatomy, Cumming School of Medicine,
25 University of Calgary, Calgary, AB Canada; [9]Hotchkiss Brain Institute,
26 University of Calgary, Calgary, AB Canada; [10]Canada Research Chair in
27 Mitochondrial Signaling and Physiopathology, Department of Biology, University
28 of Moncton, NB Canada; [11]Department of Research and Development, IMG
29 Pharma Biotech S.L., Derio, Spain; [12]Alberta Children's Hospital Research
30 Institute, University of Calgary, Calgary, AB Canada; [13]Biocruces Bizkaia Health
31 Research Institute, Barakaldo, Spain; [14]Division of Medical Sciences, University of
32 Victoria, Victoria, BC, Canada.

33
34 [15] These authors contributed equally

35 [16] Senior Authors

36 [17] Lead Contact

1 *Correspondence to: Edgar Soria-Gomez, edgar.soria@achucarro.org

2 Luigi Bellocchio, luigi.bellocchio@inserm.fr

3 Giovanni Marsicano, giovanni.marsicano@inserm.fr

SUMMARY

5 Recent advances in neuroscience positioned brain circuits as the key units

6 controlling behavior, implying that their positive or negative modulation

7 necessarily leads to specific behavioral outcomes. However, emerging evidence

8 suggests that activation or inhibition of specific brain circuits can actually

9 produce multimodal behavioral outcomes. Here we show that, in the same

10 neuronal circuit, activation of a receptor at different subcellular locations can

11 determine distinct specific behaviors. Pharmacological activation of type-1

12 cannabinoid receptors (CB_1) in the striatonigral circuit elicits both antinociception and

13 catalepsy in mice. The reduction of nociception depends on the activation of plasma

14 membrane-residing CB_1 receptors ($pmCB_1$), leading to inhibition of PKA activity and

15 Substance-P release. Conversely, mitochondrial-associated CB_1 receptors ($mtCB_1$)

16 located at the same terminals mediate cannabinoid-induced catalepsy through decrease

17 of intra-mitochondrial PKA-dependent cellular respiration and synaptic transmission.

18 Thus, subcellular-specific CB_1 receptor signaling within striatonigral circuits

19 determines multimodal control of behavior.

1 INTRODUCTION

2 The cannabinoid receptor type-1 (CB_1) is the main target of cannabinoid

3 compounds. Cannabinoids possess high therapeutic potentials (Cohen et al.,

4 2019), particularly in the management of pain sensitivity (Donvito et al., 2018).

5 However, because of significant side-effects (e.g., cognitive and motor

6 dysfunctions; Borgelt et al., 2013; Prashad and Filbey, 2017) their medical and

7 recreational use is under intense scrutiny (Cohen et al., 2019). In particular,

8 activation of CB_1 receptors impairs motor control (Giuffrida and Seillier, 2012;

9 Monory et al., 2007) and cataleptic-like effects are considered the leading

10 cause of vehicle accidents caused by human cannabis consumption (Martin et

11 al., 2017).

12 Basal ganglia circuits, classically associated with motor control, are now studied

13 in different contexts, including cognition and nociception. In particular,

14 striatonigral circuits formed by dopamine receptor type-1 (D_1)-positive striatal

15 medium spiny neurons projecting to the substantia nigra pars reticulata (SNr)

16 play crucial roles in motor regulation (Freeze et al., 2013) and participate in

17 nociception (Taylor et al., 2016). Indeed the SNr represents the ideal hub

18 coordinating voluntary movement and nociceptive responses according to the

19 different inputs received (Zhou et al., 2016), and displays one of the highest

20 levels of CB_1 receptor protein expression in the brain (Marsicano and Kuner,

21 2008).

22 Neuronal CB_1 receptors are predominantly associated with presynaptic terminal

23 plasma membranes (pmCB_1; Ibsen et al., 2017) and their activation mainly

results in the fine-tuned regulation of neurotransmitter and neuropeptide release (Busquets-Garcia et al., 2018). However, recent data indicate that functional CB_1 receptors are also present in intracellular compartments, particularly in association with mitochondria ($mtCB_1$; Benard et al., 2010; Busquets-Garcia et al., 2018; Hebert-Chatelain et al., 2016; Jimenez-Blasco et al., 2020; Koch et al., 2015), where they modulate bioenergetic and memory processes (Hebert-Chatelain et al., 2016). Indeed, normal mitochondrial functions are required for proper synaptic transmission underlying behavioral control (Francisco et al., 2020; Kanellopoulos et al., 2020; Rangaraju et al., 2014).

The double subcellular functional localization of CB_1 receptors in striatonigral circuits suggests that cannabinoids might exert different effects not only by altering the functions of different cell types and brain circuits, but also by impacting different subcellular processes within the same circuits. Thus, here we used the diverse distribution of CB_1 receptors as a tool to investigate whether subcellular constraints in the same neuronal circuit can determine multimodal behavioral control.

RESULTS

Striatonigral CB_1 receptors mediate cannabinoid-induced motor impairments and antinociception

Cannabinoid agonists dose-dependently decrease motor activity and induce antinociception through the activation of central CB_1 receptors (Metna-Laurent et al., 2017; Monory et al., 2007). To test whether CB_1 receptor signaling in the SNr is responsible for these effects, we locally infused (**Figure S1A**) the CB_1

receptor-selective antagonist AM251 in mice systemically treated (intraperitoneal, i.p.) with the plant-derived CB_1 receptor agonist Δ^9-tetrahydrocannabinol (THC, 10 mg/kg). AM251 fully blocked the THC-induced reduction in locomotor activity in the open field (**Figure S1B**), catalepsy in the horizontal-bar test (**Figure 1A**) and antinociception in the hot-plate test (**Figure 1B**), indicating that activation of CB_1 receptors in this brain region is necessary for these effects. As a control, voluntary or accidental misplacement of the cannulas to brain areas just adjacent to the SNr (**Figure S1A**) eliminated any impact of AM251 on THC-induced catalepsy, antinociception or hypolocomotion (**Figure 1A, 1B and S1B**), clearly indicating the local specificity of the effect.

The SNr receives direct (striatonigral) and indirect (striatopallidal - pallidonigral) information from striatal medium spiny neurons (MSNs). MSNs belonging to the direct pathway preferentially express dopamine D_1R receptor, whereas the indirect pathway ones are identified by the expression of dopamine D_2R receptor, although in the external segment of the Glubus Pallidus (GPe) there are some collateral D_1R-positive projections (Freeze et al., 2013). Interestingly, CB_1 receptors are abundantly expressed by both neuronal populations (Fernandez-Ruiz et al., 2011). To identify which subpopulation of CB_1 receptors are responsible for the antinociceptive and motor effects of THC, we used an intersectional recombinase approach (Zhao et al., 2020). We injected a recombinant adeno-associated virus (rAAV) expressing the Cre recombinase protein in a flipase (FLP)-dependent manner (AAV-FRT-iCre-EGFP) in the striatum of mice carrying a "floxed" CB_1 gene (*CB_1*-flox; Marsicano et al., 2003). Simultaneously, a retrograde rAAV expressing flipase (AAV-retro-FLP-BLFP)

1   was administered into either the GPe or the SNr (**Figure S1C**). Thus, we

2   obtained the expression of the Cre recombinase in striatopallidal or striatonigral

3   neurons of CB_1-flox mice, leading to the generation of ST-GP-CB_1-KO or ST-

4   SN-CB_1-KO mutants that carrying the deletion of the receptor gene in either

5   populations, respectively (**Figure S1C**). *In situ* hybridization coupled to GFP

6   immunostaining for Cre detection showed that the recombinase was

7   preferentially expressed in D_1R neurons over D_2R in ST-SN-CB_1-KO (D_1R/Cre

8   cells 68.5±2.8%; D_2R/Cre cells 9±1%) with an opposite situation in ST-GP-CB_1-

9   KO (D_1R/Cre cells 21.7±1.9%; D_2R/Cre cells 42.5±5.1%).

10 Deletion of CB_1 receptor gene in these models was confirmed by double *in situ*

11 hybridization experiments, which showed preferential loss of CB_1 receptor

12 expression by D_1R-expressing striatal neurons in ST-SN-CB_1-KO mice and by

13 D_2R expressing neurons in the ST-GP-CB_1-KO mice (**Figure S1D**). Accordingly,

14 ST-SN-CB_1-KO showed a consistent reduction of CB_1 immunoreactivity in the

15 SNr whereas in ST-GP-CB_1-KO, CB_1 protein was selectively reduced in the

16 GPe (**Figure 1C)**.

17 Whereas ST-GP-CB_1-KO mice responded to THC treatment similar to control

18 animals, ST-SN-CB_1-KO littermates did not display either catalepsy or

19 antinociception upon THC administration (**Figure 1D and 1E**). On the other

20 hand, the hypolocomotor effect of THC was maintained upon both

21 manipulations (**Figure S1E**), suggesting that other subpopulations of SNr CB_1

22 receptors are likely involved in this effect. These data indicate that activation of

23 CB_1 receptors expressed at striatonigral, but not striatopallidal, terminals is

1 necessary for THC-induced antinociception and catalepsy, revealing a common

2 anatomical target for these effects.

3

Cannabinoid-induced antinociception relies on activation of striatonigral pmCB$_1$ and regulation of Substance-P/NK$_1$ receptor activity

7 THC and AM251 are lipophilic molecules, which easily cross biological

8 membranes, thereby potentially acting at both plasma membrane and

9 intracellular CB$_1$ receptors. To distinguish between the contributions of these

10 two pools of CB$_1$ receptors to the THC effects in the SNr, we locally

11 administered the CB$_1$ receptor antagonist Hemopressin (Hp; Heimann et al.,

12 2007). Hp is a peptide compound, which is unable to cross the plasma

13 membrane (Benard et al., 2012) and, thereby, antagonizes only pmCB$_1$

14 receptors but not intracellular ones (Benard et al., 2012; Rozenfeld and Devi,

15 2008). Intra-SNr administration of Hp did not exert any effect by itself and it was

16 not able to reverse THC-induced catalepsy (**Figure 1F**), but it strongly reduced

17 the antinociceptive effect of THC (**Figure 1G**). Striatonigral neurons are known

18 to release several neuropeptides, including Substance-P (Deniau et al., 2007;

19 Johnson et al., 2016), which promotes pain perception *via* central activation of

20 its main target, the type-1 neurokinin receptor (NK$_1$; Steinhoff et al., 2014).

21 Interestingly, inhibition of NK$_1$ signaling can decrease pain reactions induced by

22 systemic CB$_1$ receptor blockade (Darmani and Pandya, 2000), and some

23 evidence suggests a negative role of CB$_1$ receptor signaling in Substance-P

1 production and release in the spinal cord and the striatum (Lever and

2 Malcangio, 2002; Steiner et al., 1999). To test whether Substance-P signaling in

3 the SNr might underlie THC-induced antinociception, we systemically

4 administered the selective NK_1 receptor agonist GR73632 (Ray et al., 2009), in

5 combination with THC. GR73632 (75 µg/kg) alone had no effect in any test, and

6 it did not alter the cataleptic effect of THC (**Figure S1F**). However, this

7 treatment blocked the antinociceptive effect of the cannabinoid (**Figure S1G**).

8 Then, in order to verify that the interaction between CB_1 and NK_1 receptors

9 occurs in the SNr, GR73632 was locally injected before systemic THC

10 treatment. This treatment did not alter THC-induced catalepsy (**Figure 1H**), but,

11 strikingly, it fully abolished the antinociceptive effect of THC (**Figure 1I**). These

12 data show that cannabinoid-induced antinociception involves Substance-P

13 signaling, suggesting that activation of CB_1 receptors might reduce the release

14 of the neuropeptide at striatonigral terminals. To test this hypothesis, we

15 established an *ex vivo* "sniffer cells" approach (**Figure S1H**), which has been

16 already successfully used to detect the release of other neuropeptides in real

17 time (Zaelzer et al., 2018). We transfected HEK-293T cells with 2 plasmids for

18 co-expression of NK_1 receptor together with the calcium indicator GCaMP6s

19 (**Figure S1H**) to obtain cells capable of detecting exogenously applied

20 Substance-P in a very sensitive (EC50, 5.1 nM) and specific way (**Figure S1H**

21 **and S1I**). These cells were then seeded over acute sagittal brain slices

22 containing the striatonigral pathway (**Figure 1J**). After 2-hour rest to allow

23 cellular adhesion to the slices, GCaMP6s fluorescence was imaged (Zaelzer et

24 al., 2018) (**Figure 1J**) before and after electrical stimulation of the striatonigral

25 afferents. This manipulation elicited a marked increase in GCaMP6s

fluorescence in cells placed above the SNr (**Figure 1K, S1J, S1K, S1L, S1M**), indicating an increase in Substance-P release. The increase in fluorescence is specific for the peptide, since is absent when slices are treated with cells only expressing GCaMP6s (**Figure S1J and S1L**) and it was blocked by the NK_1 selective antagonist CP122721 (**Figure S1K and S1L**). Strikingly, application of the cannabinoid agonist WIN55,212-2 (WIN) dramatically reduced electrically evoked Substance-P release in wild type mice (**Figure 1K and S1M**), but not in *CB_1*-KO littermates (**Figure 1K**). WIN did not affect the response to exogenous peptide (**Figure S1N**), showing that its effect in slices was due to a CB_1 receptor-mediated decrease of Substance-P release.

To further confirm the striatonigral origin of Substance-P release as well as its modulation by cannabinoids, we coupled the sniffer cells approach to optogenetic stimulation (Zaelzer et al., 2018). For this aim, we virally expressed the red-activated channelrhodopsin ChrimsonR (Klapoetke et al., 2014) in D_1R-Cre positive cells (Lemberger et al., 2007) of the striatum and then we conducted sniffer experiments in SNr slices (**Figure 1L**). As technical validations of the approach, we also performed patch clamp experiments in SNr neurons upon light stimulations. As expected based on the partial spectrum overlapping of the used light wavelength (Klapoetke et al., 2014), the application of the blue light to record calcium levels in the sniffer cells induced a slight activation of Chrimson and triggered-GABAergic currents which, however, had a much lower amplitude than the ones triggered by the red light (**Figure S1O**). Thus, some experiments had to be discarded because the blue-light stimulation was able to saturate the subsequent red-light-induced Substance-P

release. Nevertheless, Chrimson activation by red-light triggered above-baseline calcium responses in sniffer cells in approximately 50% of the experiments. In these conditions, calcium responses indicating Substance-P release were drastically reduced by the application of WIN (**Figure 1M**), similarly as previously observed with electrical stimulation.

Altogether, these data indicate that $pmCB_1$ receptors at D_1R-positive striatonigral terminals are responsible for THC-induced antinociception, involving the modulation of Substance-P/NK_1 signaling. Additionally, these results point out a different mechanism for the cataleptic effect, which likely involves intracellular CB_1 receptors in the SNr.

Subcellular localization of CB_1 receptors in the SNr

To investigate the intracellular distribution of the CB_1 receptor in the SNr, we used immunogold electron microscopy (Puente, 2019). The majority of CB_1 receptor protein in the SNr of WT mice was associated to the plasma membrane ($pmCB_1$) of synaptic terminals (**Figure 2A-C and S2A**). Quantifications of gold particles using stringent parameters to identify mitochondrial-localized immunoreactivity (Puente, 2019) revealed that CB_1 receptors in the SNr are anatomically associated to mitochondrial membranes ($mtCB_1$) with a density of approximately 3 particles per 20 μm^2 (**Figure 2A-D and S2A**). Moreover, approximately 10% of total mitochondria analyzed were labeled with CB_1 receptor in WT mice (**Figure 2A-E and S2A**). Conversely, only background levels of CB_1 immunoreactivity was detected in any analyzed compartment of *CB_1*-KO mice (**Figure 2A-E and S2A**), clearly demonstrating the existence of $mtCB_1$ in striatonigral terminals.

Generation of DN22-CB_1-KI mutant mice, lacking mtCB$_1$ receptors

We previously showed that a mutant version of the CB$_1$ protein lacking the first 22 amino acids (called DN22-CB$_1$) is neither anatomically nor functionally associated to mitochondrial membranes, nevertheless maintaining its other functions (e.g. at plasma membrane; Hebert-Chatelain et al., 2016). Thus, we generated a new knock-in mutant mouse line (called DN22-CB_1-KI; Pagano Zottola et al., 2020), in which the wild-type CB_1 receptor gene is replaced by the coding sequence of the DN22-CB$_1$ protein (**Figure S2B**). Quantifications of CB$_1$ receptor mRNA (by qRT-PCR) and protein (by immunofluorescence) revealed no significant differences between WT and DN22-CB_1-KI mice in many different brain regions (**Figure S2C and S2D**). Counting of gold particles in immuno-electron microscopy experiments indicated that the total amount of CB$_1$ receptor protein in the SNr was not significantly different between DN22-CB_1-KI and WT littermates (**Figure 2F, 2G and S2D**). Similarly, the levels of pmCB$_1$ were not impacted by the mutation (**Figure 2F, 2H and S2D**). However, the density of mitochondrial-associated mtCB$_1$ receptors and the percentage of CB$_1$-positive mitochondria were significantly lower in DN22-CB_1-KI mice as compared to WT littermates, reaching levels undistinguishable from global CB_1-KO mice (**Figure 2F, 2I, 2J and S2D**). To test the ability of DN22-CB$_1$ receptors to activate G protein signaling, we performed [^{35}S]GTPγ binding assays upon stimulation with the cannabinoid agonist WIN in cortical, hippocampal and midbrain extracts from WT, CB_1-KO, and DN22-CB_1-KI mice (**Figure 2K**). The DN22-CB$_1$ mutant was as efficient as its wild-type cognate in triggering G protein activation (**Figure 2K**). These results were also confirmed by *in situ* [^{35}S]GTPγ binding assays in other brain regions (**Figure S2E and S2F**). Moreover,

1   autoradiographic analyses of [^{3H}]CP55.940 cannabinoid agonist binding in

2   parallel sections did not identify any significant difference between the two

3   genotypes (**Figure S2G and S2H**). Thus, DN22-*CB$_1$*-KI mice display normal

4   binding of cannabinoid ligands and subsequent activation of G-protein

5   signaling.

6   Oxygen consumption assays in substantia nigra (SN) homogenates revealed

7   that WIN lowered ADP-stimulated mitochondrial respiration in WT but not in

8   *CB$_1$*-KO mice (**Figure 2L and S2I**), indicating a specific CB$_1$-mediated control of

9   mitochondrial activity. Notably, this effect was also abolished in SN

10   homogenates from DN22-*CB$_1$*-KI mice, showing its dependency on mtCB$_1$

11   receptors (**Figure 2L and S2I**). The DN22-*CB$_1$*-KI mutant strain was viable,

12   fertile and presented normal body weight, muscular strength and locomotion

13   (**Figure S3A and S3B**). Interestingly, DN22-*CB$_1$*-KI mice did not display any

14   alteration in voluntary running wheel activity (**Figure S3C**), where global *CB$_1$*-

15   KO mice are impaired (Dubreucq et al., 2010), showing that certain CB$_1$

16   receptor-dependent behavioral functions are maintained in these mutants.

17   Previous evidence suggests that mtCB$_1$ receptors might be partly responsible

18   for electrophysiological depolarization-induced suppression of inhibition in the

19   hippocampus (DSI; Benard et al., 2012), which is known to depend on

20   endocannabinoid signaling (Wilson et al., 2001). Interestingly, DN22-*CB$_1$*-KI

21   mice displayed DSI, but its amplitude was slightly decreased as compared to

22   WT littermates (**Figure S3D and S3E**), confirming the participation of mtCB$_1$

23   receptors in this form of synaptic plasticity (Benard et al., 2012). Altogether,

24   these observations indicate that the constitutive deletion of the first 22 amino

1 acids of the CB_1 protein specifically impacts the effects of cannabinoids

2 involving mitochondrial activity, but leave other functions of CB_1 receptors

3 unchanged. Therefore, DN22-CB_1-KI mutant mice represent a novel and

4 suitable tool to untangle the roles of mtCB_1 receptors.

5

6 Activation of mtCB_1 receptors decreases synaptic transmission

7 at striatonigral terminals and induces catalepsy, but not

8 antinociception

9 To explore if mtCB_1 receptors participate in the well-known cannabinoid control

10 of synaptic transmission in the SNr (Sales-Carbonell et al., 2013; Szabo et al.,

11 2000), we performed optogenetic-coupled electrophysiological recordings of

12 striatonigral neurotransmission in slices. The rAAV expressing

13 channelrhodopsin (Chr2) under the neuronal synapsin promoter (AAV-synP-

14 Chr2-mCherry) was injected into the dorsal striatum (**Figure 3A**) of DN22-CB_1-

15 KI, CB_1-KO mice and WT littermates. Non-dopaminergic neurons receiving

16 Chr2-expressing fibers from striatonigral projecting neurons were recorded

17 using whole-cell patch clamp in SNr slices (**Figure 3B**). Delivery of brief light-

18 pulses on striatonigral terminals triggered reliable optically-induced inhibitory

19 post-synaptic currents (oIPSCs) in SNr neurons, which were sensitive to $GABA_A$

20 blockade (**Figure 3C**). Treatment with WIN (5 µM) reduced oIPSCs in WT but

21 not in CB_1-KO mice (**Figure 3D and 3E**), suggesting a CB_1-dependendent

22 mechanism. Interestingly, WIN-mediated reduction of oIPSCs was absent in

23 slices from DN22-CB_1-KI mice (**Figure 3D and 3E**). Furthermore, no changes

were observed in the paired-pulse ratio during baseline, indicating a normal synaptic efficiency in DN22-CB_1-KI mice as compared to their WT littermates (**Figure S3F**). These data indicate that mtCB$_1$ receptors are necessary for the cannabinoid-induced inhibition of synaptic transmission in the striatonigral pathway, which has been proposed as a potential mechanism for cannabinoid-induced catalepsy (Garcia et al., 2016). Accordingly, THC or WIN administrations induced strong catalepsy in WT mice, but not in DN22-CB_1-KI littermates (**Figure 3F**). Conversely, both genotypes displayed normal cannabinoid-induced antinociception (**Figure 3G**). Interestingly, WIN application reduced Substance-P release in DN22-CB_1-KI SNr slices (**Figure S3G**) to a similar extent as observed in WT slices (**Figure 1K**). Furthermore, both intra-SNr hemopressin infusion (**Figure S3H**), as well as systemic administration of the NK$_1$ receptor agonist GR73632 (**Figure S3I**) strongly reduced THC-induced antinociception in DN22-CB_1-KI mice. Therefore, the CB$_1$-dependent control of Substance-P release in the SNr, and subsequent antinociceptive effect, do not require mtCB$_1$ receptors. These data show that the activation of mtCB$_1$ receptors is necessary for cannabinoid-induced synaptic depression in the SNr and catalepsy. Conversely, mtCB$_1$ receptors are dispensable for the local cannabinoid-induced signaling leading to antinociception. Thus, a mechanistic double dissociation of these effects of cannabinoids seems to exist in the SNr.

1 **Cannabinoid-induced catalepsy relies on activation of**

2 **striatonigral mtCB$_1$ receptors and mitochondrial inhibition**

3 Striatal dopamine receptor type-1 (D$_1$)-positive cells are one of the major

4 components of striatonigral circuits (Freeze et al., 2013). Notably, mice lacking

5 the *CB$_1$* gene in D$_1$-positive cells (D$_1$-*CB$_1$*-KO) do not display cannabinoid-

6 induced catalepsy (Monory et al., 2007). We took advantage of this phenotype

7 to investigate the specific impact of striatonigral mtCB$_1$ receptor activation on

8 the cataleptic effect of cannabinoids. For this purpose, we adopted a CB$_1$

9 rescue approach (**Figure 4A**) by injecting Cre-dependent viral vectors

10 expressing CB$_1$ or DN22-CB$_1$ (AAV-DIO-CB$_1$ or AAV-DIO-DN22-CB$_1$,

11 respectively) directly into the dorsal striatum of D$_1$-*CB$_1$*-KO mice (expressing

12 Cre specifically in D$_1$ positive cells) to specifically target striatonigral neurons

13 (**Figure 4B and 4C**). Oxygen consumption assays revealed that WIN failed to

14 decrease mitochondrial respiration in SN extracts from D$_1$-*CB$_1$*-KO mice

15 injected with a control virus (**Figure 4D**). The re-expression of CB$_1$ receptors in

16 striatal D$_1$-positive cells of mutant mice fully rescued the cannabinoid-induced

17 decrease of oxygen consumption in the SN (**Figure 4D**), whereas the injection

18 of AAV-DIO-DN22-CB$_1$ was not able to restore this effect (**Figure 4D**). The

19 rescue of CB$_1$ receptors in striatonigral cells was sufficient to restore the

20 cataleptic effect of THC in D$_1$-*CB$_1$*-KO mice (**Figure 4E**). In contrast, no

21 catalepsy was observed after DN22-CB$_1$ expression in THC-treated D$_1$-*CB$_1$*-KO

22 mice (**Figure 4E**). Additionally, we performed correlation analysis between the

23 levels of CB$_1$ expression (**Figure 4C**) and THC-induced catalepsy (**Figure 4E**)

24 in mice with rescue of CB$_1$ or DN22-CB$_1$. The absence of positive correlation

(**Figure S3J**) between the parameters, indicates that the subcellular localization rather than the expression levels of CB_1 determines the cataleptic effect of cannabinoids.

Thus, $mtCB_1$ receptor signaling in the striatonigral circuit is responsible for the local reduction of mitochondrial respiration and the cataleptic effect induced by cannabinoids.

Cannabinoid-induced catalepsy involves striatonigral mitochondrial sAC activity

To identify the molecular machinery linking the effects of cannabinoids on SN mitochondrial respiration and catalepsy, we aimed at dissecting the intramitochondrial signaling pathways involved. Stimulation of $mtCB_1$ receptors activates intra-mitochondrial $G\alpha_i$ proteins, thereby inhibiting soluble adenylyl cyclase (sAC) and protein kinase-A (PKA) activities (Hebert-Chatelain et al., 2016). The cannabinoid-induced reduction of mitochondrial respiration in SN extracts was abolished by pretreatment with the sAC inhibitor KH7 (**Figure 4F**), suggesting that sAC activity is involved in $mtCB_1$ receptor-dependent effects in this brain region. On the other hand, pre-treatment with the NK_1R agonist GR73632 did not impact the effect of WIN on SN respiration (**Figure S3K**), suggesting dissociation between the two pathways. To investigate whether the intra-mitochondrial sAC pathway participates in the SNr-dependent behavioral effects of THC, we first locally injected KH7 before systemic THC treatment. The sAC inhibitor blocked the cataleptic effect of THC (**Figure 4G**), without

16

1   impacting the behavior of mice in the hot-plate test (**Figure 4H**). Thus, similarly

2   to the impact on mitochondrial respiration, the cataleptic effect of THC requires

3   sAC activity in the SNr. However, these results do not show that the CB_1

4   signaling involved in catalepsy is specific of striatonigral neurons. Since sAC

5   expression is not limited to mitochondria and KH7 can have additional targets

6   (Valsecchi et al., 2014), pharmacological experiments cannot provide definitive

7   information about the subcellular location and the molecular specificity of the

8   observed effects. To address these issues, we used a Cre-dependent viral

9   approach to overexpress a mitochondrial-targeted version of sAC (mt-sAC-HA;

10   Hebert-Chatelain et al., 2016; Valsecchi et al., 2014) that was previously

11   reported to be targeted to mitochondria (**Figure S3L**, Pearson's coefficient

12   0.70±0.04; Hebert-Chatelain et al., 2016) and block respiratory effects of

13   cannabinoids in cell cultures (Hebert-Chatelain et al., 2016). Striatonigral

14   overexpression of mt-sAC obtained by injecting AAV-DIO-mt-sAC-HA into the

15   dorsal striatum of D_1-Cre mice (Lemberger et al., 2007) (**Figure S3M and N**)

16   fully blocked the cannabinoid effect on mitochondrial respiration in SN extracts

17   (**Figure 4I and S3O**). Strikingly, these mice did not present any cataleptic effect

18   upon THC administration as compared to control mice (**Figure 4J**), whereas

19   they displayed a normal THC-induced antinociception (**Figure 4K**). These data

20   show that inhibition of intra-mitochondrial sAC signaling in striatonigral terminals

21   is not involved in antinociception, but it underlies the cannabinoid-induced

22   decrease of mitochondrial respiration and the subsequent cataleptic effect.

23

1 PKA signaling mediates both cannabinoid-induced catalepsy

2 and antinociception, but in different subcellular compartments

3 Adenylyl cyclase activity triggers several signaling pathways and the activation

4 of PKA is one of the most prominent (Dwivedi and Pandey, 2008). Inhibition of

5 PKA is one of the best characterized signaling mechanisms of CB_1 receptor

6 activation throughout the brain (Ibsen et al., 2017), including in striatal neurons

7 (Borgkvist and Fisone, 2007; Martinez et al., 2012). For instance, the activity of

8 this kinase is necessary for the stimulation of Substance-P release in spinal

9 cord and cultured dorsal root ganglion neurons, and this mechanism is

10 modulated by CB_1 receptors (Chen et al., 2018; Oshita et al., 2005). Within

11 mitochondria, PKA signaling following mt-sAC activation is a target for $mtCB_1$-

12 induced reduction of mitochondrial functions (Hebert-Chatelain et al., 2016).

13 Thus, PKA inhibition at different subcellular locations might mediate $pmCB_1$-

14 dependent antinociception and $mtCB_1$-dependent catalepsy, by reducing

15 Substance-P release and inhibiting mitochondrial respiration, respectively. To

16 test this hypothesis, we used constructs expressing constitutively active mutant

17 forms of PKA (Niswender et al., 2005) targeted either to the cytosol (PKA-CA,

18 myc tagged) or to the mitochondria (MLS-PKA-CA, myc-tagged, **Figure S3P**;

19 Hebert-Chatelain et al., 2016). These constructs were used to generate rAAVs

20 for Cre-dependent expression, which were injected into the dorsal striatum of

21 D_1-Cre mice. By this way, we obtained expression of these two different forms

22 of constitutively active PKA in striatonigral neurons (**Figure S3Q**). Expression of

23 PKA-CA did not alter catalepsy, but it blocked the antinociceptive effect of THC

24 (**Figure 4L and 4M**). Conversely, the expression of MLS-PKA-CA dampened

1 the cataleptic effect of THC, without changing the antinociception (**Figure 4L**

2 **and 4M**). Importantly, the expression of PKA-CA did not alter cannabinoid-

3 induced decrease of mitochondrial respiration in SN extracts, whereas MLS-

4 PKA-CA abolished this effect (**Figure 4N and S3R**). These data show that

5 inhibition of PKA activity in striatonigral neurons mediates both cataleptic and

6 antinociceptive effects of cannabinoids. However, the specific subcellular

7 location of the activity of this kinase is differentially involved in these effects.

8 Whereas intra-mitochondrial sAC-PKA signaling mediates cannabinoid-induced

9 decrease of mitochondrial respiration and catalepsy, the antinociceptive effect

10 of these drugs relies on the inhibition of cytoplasmic PKA.

11 **DISCUSSION**

12 This study reveals that the differential subcellular localization of a receptor can

13 bias the behavioral consequences of its activation in the same brain circuit. *Via*

14 the regulation of specific subcellular molecular pathways, striatonigral neurons

15 are the substrate of both adverse cataleptic and clinically-relevant

16 antinociceptive effects of cannabinoids. While stimulation of $pmCB_1$ receptors at

17 striatonigral terminals induces inhibition of nociceptive responses, presynaptic

18 $mtCB_1$ receptors in the same location are responsible for cataleptic effects of

19 cannabinoids (**Figure S4**). Mechanistically, cannabinoid-induced catalepsy

20 relies on $mtCB_1$ receptor-dependent regulation of intramitochondrial sAC/PKA

21 signaling, inhibition of mitochondrial respiration and decrease of inhibitory

22 synaptic transmission at striatonigral terminals. Conversely, antinociception

23 requires $pmCB_1$ receptor-dependent reduction of cytosolic PKA activity and

24 decrease of Substance-P/NK_1 receptor signaling (**Figure S4**).

1 The SNr, being a key part of the basal ganglia loop (Freeze et al., 2013), is

2 classically considered to provide mainly motor regulation, integrating striatal

3 pathways and regulating the activity of motor cortex through thalamic

4 projections (Borsook et al., 2010). However, the SNr also, directly and indirectly,

5 modulates the activity of several brain regions involved in pain processing such

6 as the superior and inferior colliculus, pedunculopontine nucleus (PPN), rostral

7 ventral medulla and dorsal root ganglia (Borzook et al., 2010; Zhou, 2016).

8 Moreover, several electrical and optogenetic stimulation studies revealed a

9 novel nociceptive network, e.g Subthalamic Nucleus – SNr – superior colliculus

10 and parabrachial nucleus (Luan et al., 2020; Pautrat et al., 2018). Thus, the SNr

11 is ideally placed to control voluntary movement, as wells as nociceptive

12 responses. There could be two different sets of striatonigral neurons, one

13 dedicated to nociception control (as indicated by the presence of different

14 nociceptive neurons in the SNr and the other to movement control (as already

15 extensively studied (Borzook et al., 2010). Alternatively the same neurons could

16 be involved in both effects according to the different inputs received and

17 possibly differential molecular mechanisms triggered by those inputs (Chudler

18 and Dong, 1995). In this scenario, the subcellular localization of CB_1 receptors

19 could serve as a molecular switch regulating motor control and pain perception.

20 More recently, an emerging idea started to grow in brain research about the

21 possibility that specific subcellular locations of a molecular process could trigger

22 different cellular effects (Creighton, 2011; Ilouz et al., 2017). For instance,

23 although their relative impact on behavior has not been investigated so far,

24 specific subcellular locations of targeted molecules have been proposed to

1 differentially modulate cellular processes in the same brain cells (Bucko et al.,

2 2019; Qi et al., 2019; Skalhegg and Tasken, 2000). The recent evidence that

3 certain GPCRs, including CB_1, can functionally localize to different organelles

4 (Benard et al., 2012; Eichel and von Zastrow, 2018; Hebert-Chatelain et al.,

5 2016; Lahuna and Jockers, 2018) indicates that they might be directly involved

6 in these subcellular-specific signaling pathways and their behavioral

7 consequences. Moreover, given the crucial role of proper GPCRs trafficking

8 for their activity (Lobingier and von Zastrow, 2019), one might speculate that

9 a transient mitochondrial passage might be a determinant of certain CB_1

10 functions at plasma membranes. Although not yet possible to be directly

11 addressed experimentally, this interesting hypothesis might change the current

12 view of receptor trafficking and will be for sure the subject of future studies.

13 The activation of $mtCB_1$ receptors in striatonigral terminals is responsible for the

14 effects of cannabinoids on cellular respiration, synaptic transmission and

15 behavioral catalepsy. A growing body of evidence highlights the importance

16 of mitochondrial functions for the regulation of synaptic transmission (Garcia

17 et al., 2019; Vos et al., 2010), but little is known concerning the detailed

18 molecular mechanisms linking the organelle to the synaptic machinery. The

19 constant supply of ATP produced by mitochondria is considered to be a key

20 element for sustaining synaptic transmission (Rangaraju et al., 2014). By

21 regulating mitochondrial respiration at synaptic terminals, $mtCB_1$ receptors

22 are therefore perfectly placed to potentially dampen inhibitory striatonigral

23 neurotransmission and, thereby, induce catalepsy upon pharmacological

24 activation. This suggests that similar mechanisms might occur during

physiological fine-tuned control of movements, thereby establishing a link between mitochondrial activity, synaptic transmission and motor control.

The assessment of nociception in animal models necessarily relies on the observation of motor responses. Thus, it has been proposed that cannabinoid-induced decrease of pain reactions might be secondary to motor impairments, such as catalepsy, rather than reflecting proper antinociception (Giuffrida and Seillier, 2012; Pertwee, 2001). However, analgesic and antinociceptive effects of cannabinoids have been observed at several supraspinal and spinal locations, in the absence of motor alterations, indicating that these two effects can be discriminated at the level of different brain and spinal cord regions (Woodhams et al., 2017). Our data show that both behavioral outputs can be mediated by activation of CB_1 receptors located in different subcellular organelles in striatonigral neurons, triggering distinct molecular mechanisms. This does not only add a new location for cannabinoid effects, but it also shows that CB_1 receptor-dependent catalepsy and antinociception rely on a true intracellular mechanistic dichotomy, likely involved in the physiological regulation of complex processes, such as motor and pain control. This dichotomy, observed after acute pharmacological activation of CB_1 receptor, might be also underlying the physiological role of endogenous cannabinoids in motor regulation and pain processing. Indeed, pharmacological and/or genetic CB_1 receptor blockade increases the sensitivity to pain perception (Clapper et al., 2010; Nadal et al., 2013) and also have been often reported to increase locomotor reactivity (Griebel et al., 2005; Häring et al., 2011). On the other hand, like THC and other cannabinoid agonists, inhibitors of endocannabinoids

degradation are able to induce antinociception and catalepsy via CB_1 receptor activation (Long et al., 2009), further confirming the endogenous role of the receptor in regulating these two physiological processes.

Cannabinoids induce antinociception through the $pmCB_1$ receptor-dependent reduction of Substance-P release in striatonigral neurons and the consequent decrease of local NK_1 receptor signaling. Interestingly, Substance-P in the SNr participates in pain processing, possibly through the modulation of the activity of rostral ventral medulla and dorsal root ganglia(Boccella et al., 2020; Borsook et al., 2010; Taylor et al., 2016). Therefore, the CB_1 receptor-dependent modulation of Substance-P/NK_1 signaling in the striatonigral neurons is a novel mechanism that likely participates in larger circuits modulating nociceptive responses.

To conclude, CB_1 receptors in the striatonigral circuit mediate cannabinoid-induced catalepsy and antinociception. This regulation clearly involves distinct subcellular and molecular mechanisms in the same neuronal circuit, resulting in the respective control of neurotransmitter and neuropeptide release. Thus, selective subcellular manipulations of CB_1 receptors represent a potential therapeutic strategy to avoid undesirable effects of cannabinoid drugs, and to promote their beneficial pain treatment. The unforeseen dichotomy between cannabinoid-induced mitochondrial catalepsy and non-mitochondrial antinociception in the same cellular population introduces the concept of subcellular specificity of behavioral control.

24

AUTHOR CONTRIBUTIONS

E.S-G., and L.B., performed and analyzed behavioral, biochemical and anatomical experiments. A.C.P.Z., C.M., M.L.B-J., R.F., I.M.M., Y.O.A., A.C., T.L-L., P.V., T.T-C., J.S.B., E.H-C., G.B-G., A.W.L., and L.F.C. performed and analyzed biochemical experiments. Y.M., T.D., L.M.R., J.F.C.O., S.C., J.C., L.M., B.R., A.B-G., and F.C., performed and analyzed behavioral experiments. M.B., G.T., and J.B., performed and analyzed electrophysiological experiments. Y.M., I.B-d-R., M.V., Z.Z., F.J-K., N.P., and P.G., performed and analyzed anatomical experiments. E.S-G., G.M., and L.B., conceived and supervised the whole project and wrote the manuscript. All authors edited and approved the manuscript.

DECLARATION OF INTERESTS

The authors declare no competing interests.

1 **STAR METHODS**

2 **Animals**

3 Experiments were approved by the Committee on Animal Health and Care of

4 INSERM, and the French Ministry of Agriculture and Forestry (authorization

5 number 3306369). Mice were maintained under standard conditions (food and

6 water *ad libitum*; 12h/12h light/dark cycle, light on 7 a.m.; experiments were

7 performed between 9 a.m. and 5 p.m.). C57BL/6-N male mice (2–4 months old)

8 were purchased from Janvier (France). D_1-CB_1-KO mice and their WTs

9 littermates were generated and maintained as previously described(Monory et

10 al., 2007). D_1-Cre mice(Lemberger et al., 2007) were kindly provided by

11 Günther Schütz, (German Cancer Research Center). DN22-CB_1-KI mice were

12 generated using a flox-stop strategy as previously described(Ruehle et al.,

13 2013). Stop cassette was excised *via* a Cre deleter mouse strain and knock-in

14 mice were maintained over a C57BL6/N background for several generations

15 before experiments.

16 **Drugs**

17 THC was obtained from THC Pharm GmbH (Frankfurt, Germany). AM251,

18 Hemopressin and GR73632 were purchased from Tocris (France). WIN 55,212-

19 2 mesylate salt and KH7 were obtained from Sigma Aldrich (France). THC

20 (10mg/kg) was dissolved in a mixture of saline (0.9% NaCl) with 5% ethanol

21 and 4% cremophor. WIN 55,212-2 was dissolved in DMSO for *in vitro*

22 experiments and in mixture of DMSO, Tween80 (1.25-1.25-97.5) and saline for

23 *in vivo* treatments. Hemopressin (22 ng in 0.5 µl) and GR73632 (100ng in 0.5µl)

24 were dissolved in saline. AM251 (4 µg in 0.5µl) and KH7 (2µg in 0.5µl) were

1 dissolved in 10% DMSO, 10% cremophor and 80% saline. Vehicles contained

2 the same amounts of solvents respectively to the drug. All drugs were prepared

3 fresh before the experiments.

4 **Viral vectors**

5 To generate AAV-DIO-CB$_1$, AAV-DIO-DN22, AAV-DIO-mt-sAC-HA, AAV-DIO-

6 PKA-CA and AAV-DIO-MLS-PKA-CA the coding sequences for the 5

7 proteins(Hebert-Chatelain et al., 2016) were subcloned in pAAV-CAG-flex

8 plasmid (kindly gifted by Matthias Klugmann, UNSW, Australia) by using

9 standard molecular cloning techniques. The same pAAV-CAG-flex plasmid was

10 used as empty control (AAV-DIO-ctr). AAVs were generated by PEI transfection

11 of HEK 293T cells and purified by iodixanol-gradient ultracentrifugation as

12 previously described(Hebert-Chatelain et al., 2016). Virus titers were 5.43×10^{11}

13 for AAV-DIO-CB$_1$, 3.34×10^{11} for AAV-DIO-DN22, 2.36×10^{11} for AAV-DIO-mt-

14 sAC-HA, 3.87×10^{11} for AAV-DIO-PKA-CA, 3.96×10^{11} for AAV-DIO-MLS-PKA-CA

15 and 4.51×10^{11} for AAV-DIO-ctr, expressed as genomic copies (GC) x ml.

16 For optogenetic experiments, rAAV2-hSyn-ChR2(H134R)-mCherry (10^{13}

17 GCxml) and rAAV-hSyn-DIO-ChrimsonR-tdTomato (5.2×10^{12} GCxml) were

18 purchased from UNC vector core (USA) and Viral Vector Facility (VVF) of the

19 Neuroscience Center Zurich (Zentrum für Neurowissenschaften Zürich, ZNZ)

20 respectively.

21 The viral vectors used for CB$_1$ deletion experiment (*see next section*) were

22 purchased from the VVF. Titres were: 6.4×10^{12} for AAV-retro-hSyn1-EBFP2-

23 FLPo, 4.1×10^{12} for AAV-retro-hSyn1-EBFP2 and 6.3×10^{12} for AAV-hEF1a-dFRT-

24 iCre-EGFP.

Surgery and drug/virus administration

For intra-SNr injections of drugs mice were anesthetized by intraperitoneal injection of a mixture of ketamine (100mg/kg, Imalgene 500®, Merial) and Xylazine (10mg/kg, Rompun, Bayer) and placed into a stereotaxic apparatus (David Kopf Instruments) with mouse adapter and lateral ear bars. Mice were allowed to recover for at least one week in individual cages before the beginning of the experiments. Mice were weighed daily and individuals that failed to regain the pre-surgery body weight were excluded from the following experiments. Mice were bilaterally implanted with 3.5 mm stainless steel guide cannulae (Plastics One, USA) targeting the SNr with the following coordinates: AP -3.2, L ± 1.3, DV –3.5, according to Paxinos and Franklin(Paxinos and Franklin, 2001). Guide cannulae were secured with cement anchored to the skull by screws. The drug injections for intra-SNr were performed by using injectors protruding 1 mm from the tip of the cannula. The correct placement of the SNr cannulas was verified by injection of sky-blue toluidine followed by neutral red staining(Soria-Gomez et al., 2014) (**Figure S1A**).

AAV injections of AAV-DIO-CB_1 or AAV-DIO-DN22 in the dorsal striatum of D_1-*CB_1*-KO mice, or AAV-DIO-mt-sAC-HA, AAV-DIO-PKA-CA and AAV-DIO-MLS-PKA-CA in D_1-Cre mice, with respective AAV-DIO-Ctr, were performed with the following coordinates: AP +0,5 L ± 2,0, DV –3.0 as previously described(Bellocchio et al., 2016).

For the specific deletion of CB1 in the striatopallidal or striatonigral neurons, mice were anesthetized by inhalation of isofluorane 5% and placed into the stereotaxic apparatus with the anesthesia maintained at 2% during the entire

1 surgery. AAV vectors were injected with the help of a microinjector (Nanoject III,

2 Drummond Scientific, PA, USA). The deletion was performed injecting the viral

3 vectors AAV-hEF1a-dFRT-iCre-EGFP in the dorsal striatum, STR (2 injections

4 of 1µl per side) with the following coordinates: AP + 0,8 ML ± 2,0 DV -3,0 and -

5 3,5; and the retrogade vector AAV-retro-hSyn1-EBFP2-FLPo or AAV-retro-

6 hSyn1-EBFP2 as control in one of its target external Globus Pallidus, GPe or

7 Substantia nigra pars reticulata, SNr (respectively AP – 0,5 ML ± 1,8 DV – 4,25;

8 volume 350 nl per side and AP – 3,25 ML ± 1,35 DV – 4,5; volume 750 nl per

9 side).

10 Animals were allowed to recover for at least four weeks before the beginning of

11 biochemical (see after) or behavioral experiments. Mice that underwent

12 behavioral experiments were fixed by transcardial perfusion of 4% PFA and

13 their brain were processed for imaging (to detect BFLP and EGFP) and double

14 fluorescent in-situ hybridization (see below), or for immunofluorescence as

15 previously described (Hebert-Chatelain et al., 2016), with primary antibodies

16 directed against CB_1 receptor (CB_1-Go-Af450-1; 2 µg/ml; Frontier Science Co.

17 Ltd), to detect CB_1 rescue and CB_1 deletion, or against HA-tag (#3724; Cell

18 Signaling Technology Danvers, MA) to confirm overexpression of mt-sAC. Mice

19 that did not fulfill histological positive criteria were excluded from the study.

20 **Double fluorescent in-situ hybridization coupled to GFP immunodetection**

21 Double FISH/GFP immunofluorescence experiments to measure the number of

22 CB_1/D_1R vs CB_1/D_2R positive striatal neurons in the deletion experiments, were

23 carried out as previously described (Oliveira da Cruz et al., 2020; Terral et al.,

24 2019). Briefly, free-floating frozen coronal sections were cut out with a cryostat

1 (30 µm, Microm HM 500M Microm Microtech) and collected in an antifreeze

2 solution and conserved at −20°C. After inactivation of endogenous peroxidases

3 and blocking with Avidin/Biotin Blocking Kit (Vector Labs, USA), sections were

4 processed with a combination of FITCH coupled riboprobe against mouse CB1

5 receptor (1:1000, prepared as described in Marsicano and Lutz, 1999) together

6 with Digoxigenin (DIG)-labeled riboprope against D1R or D2R (1:1000 Monory

7 et al., 2007). Signals were revealed with a TSA reaction using fluorescein

8 isothiocyanate (FITC)-labeled tyramide (1:80 for 12 minutes, Perkin Elmer) for

9 CB_1 receptor, or with Streptavidin-Texas Red (1:400, PerkinElmer) for D1R or

10 D2R receptor. Sense control probes were used to establish background signal.

11 After processing for FISH, anti-GFP immunofluorescence was carried out as

12 previously described (Oliveira da Cruz et al., 2020; Terral et al., 2019). Counting

13 of co-expressing cells was performed manually over 20x objective fluorescent

14 microscope as previously described (Bellocchio et al., 2010, Oliveira da Cruz et

15 al., 2020; Terral et al., 2019). Image analyses and counting was performed in at

16 least 6 striatal slice per mouse averaging results from 3-4 mice. This resulted in

17 counting 1300-1600 neurons in average per each condition/analysis.

18 **Quantitative real-time PCR (qRT-PCR).**

19 Samples from WT, DN22-CB_1-KI and CB_1-KO mice were homogenized in Tri-

20 reagent (Euromedex, France) and RNA was isolated using a standard

21 chloroform/isopropanol protocol(Chomczynski and Sacchi, 1987). RNA was

22 processed and analyzed following an adaptation of published methods. cDNA

23 was synthesized from 1 µg of total RNA using Maxima Reverse Transcriptase

24 (Thermo Scientific, USA) and primed with oligo-dT primers (Thermo Scientific,

USA) and random primers (Thermo Scientific, USA). qRT-PCR was perfomed
using a LightCycler® 480 Real-Time PCR System (Roche, Switzerland). qRT-
PCR reactions were done in duplicate for each sample, using transcript-specific
primers, cDNA (4 ng) and LightCycler 480 SYBR Green I Master (Roche,
Switzerland) in a final volume of 10 μl. The PCR data were exported and
analyzed in an informatics tool (Gene Expression Analysis Software
Environment) developed at the NeuroCentre Magendie. For the determination
of the reference gene, the Genorm method was used(Livak and Schmittgen,
2001). Relative expression analysis was corrected for PCR efficiency and
normalized against two reference genes. Valosin containing protein (Vcp) and
succinate dehydrogenase complex subunit (Sdha) genes were used as
reference genes for Amygdala. Glyceraldehyde-3-phosphate dehydrogenase
(Gapdh) and Sdha genes were used as reference genes for Hippocampus.
Tubulin alpha 4 a (Tuba4a) and tyrosine 3 mono oxygenase tryptophan 5 mono
oxygenase activation protein zeta (Ywhaz) genes were used as reference
genes for Anterior Olfactory Nucleus. Sdha and tubulin alpha 4 a (Tuba4a)
genes were used as reference genes for Prefrontal Cortex. Actin, beta (Actb)
and tTubulin alpha 4 a (Tuba4a) genes were used as reference genes for STR.
Glyceraldehyde-3-phosphate dehydrogenase (Gapdh) and peptidylprolyl
isomerase A (Ppia) genes were used as reference genes for Hypothalamus.
The relative level of expression was calculated using the comparative ($2^{-\Delta CT}$)
method(Livak and Schmittgen, 2001). Primers sequences are reported in the
following table:

Gene	GenBank ID	Forward Sequence (5'-3')	Reverse Sequence (5'-3')
Vcp	NM_009503	TGGCCGTCTAGATCAGCTCAT	TTTCGCAGATTGGCTTTTAGG
Sdha	NM_023281	TACAAAGTGCGGGTCGATGA	TGTTCCCCAAACGGCTTCT
Gapdh	NM_008084	TCAAGAAGGTGGTGAAGCAG	TGGGAGTTGCTGTTGAAGTC
Tuba4a	NM_009447	CCACTTCCCCTTGGCTACCTA	CCACTGACAGCTGCTCATGGT
Ywhaz	NM_011740	CTTGTGAGGCTGTGACACAAAC	CAAGAGTGTGCACGCAGACA
Actb	NM_007393	TGACCGAGCGTGGCTACA	CATAGCACAGCTTCTCTTTGATGTC
Ppia	NM_008907	CAAATGCTGGACCAAACACAA	GCCATCCAGCCATTCAGTCT
Cnr1	NM_007726	GTCGATCTTAGACGGCCTTGC	TTGAGCCCACGTAGAGGAGGT
Cnr1	NM_007726	GTGCTGTTGCTGTTCATTGTG	CTTGCCATCTTCTGAGGTGTG

1

2 **Mitochondrial respiration**

3 Mitochondrial respiration in substantia nigra extracts was measured as

4 previously described(Hebert-Chatelain et al., 2016) with some modification.

5 Briefly, immediately after cervical dislocation, the mouse brain was extracted

6 and the substantia nigra was rapidly dissected using the coronal brain

7 matrix(Vallee et al., 2014) and was homogenized in 450 μl of Miro5 buffer

8 without taurine supplementation (Makrecka-Kuka et al., 2015) using a Politron

9 homogenizer (11.000 rpm 3-5 sec). After brief centrifugation the supernatant

10 was treated with saponin at a final concentration of 12.5 μg/ml. Respiration

11 analyses were carried out using a 2K Oroboros device(Makrecka-Kuka et al.,

12 2015). 100 μl of lysate were put in each chamber and complex I-dependent

respiration was triggered by adding malate (2mM), pyruvate (5mM) and glutamate (10 mM) (MPG)(Makrecka-Kuka et al., 2015). Then we applied DMSO or WIN 55,212-2 at final concentration of 1μM and 5 minutes after we injected 1.25 mM ADP. Each measure of OCR in ADP condition was normalized to the values before ADP injection and the effect of WIN 55,212-2 was expressed as percentage of vehicle conditions. Only samples for which the ratio of ADP/MPG in the vehicle was equal or superior to 1.5 were retained for the analyses. In the experiments of KH7 pre-treatment, the drug was dissolved in DMSO (used as vehicle) and injected together with the lysates at a final concentration of 5µM.

In a previous set of experiments we validated the quality of mitochondria in the preparation by measuring the O_2 consumption after the MPG and ADP administration. We added the complex II substrate Succinate at the final concentration of 10mM, 10µM Cytochrome C, to check mitochondrial membrane integrity, and finally Rotenone (0.5µM) and Antimycin A (2.5µM) inhibitors of complex I and III, respectively(Makrecka-Kuka et al., 2015) (**Table S1**). When using homogenates from virus-injected mice (see above) 40ul of samples were processed for western blotting against sAC, HA-tag and myc-tag to confirm overexpression of mt-sAC and the different forms of PKA-CA in the SNr of D_1-Cre mice respectively.

Mitochondrial isolation from mouse striatum

In this set of experiments, D_1-Cre mice were injected with control AAV vector, AAV-DIO-mt-sAC-HA, AAV-DIO-PKA-CA and AAV-DIO-MLS-PKA-CA as described above. Mice were sacrificed by cervical dislocation, brains were

1 rapidly extracted and the striatum dissected on ice. Mitochondria were extracted

2 by immuno-magnetic isolation using the Mitochondrial Extraction and Isolation

3 Kits (Milteny Biotech, FRANCE) according to manufacturer instructions. After

4 tissue lysis in 1.5ml of protease inhibition buffer provided by the manufacturer,

5 one small fraction was collected as total cell lysate (TCL). Extracted

6 mitochondria and their respective TCL were re-suspended in the same buffer,

7 quantified for their protein content and loaded on polyacrylamide gel (12µg per

8 sample) for western blotting as described below.

9 **Western Blotting**

10 Protein homogenates in Miro5, added with protease inhibitors (Complete

11 protease inhibitor cocktail, Sigma-Aldrich, France) have been mixed with

12 denaturing 4x Laemmli loading buffer (250 mM Tris-HCl, 40% Glycerol, 8%

13 SDS, 5% β-Mercaptoethanol, 0.2% Bromophenol blue) and boiled at 95°C for 5

14 minutes. Samples were analyzed on 4-20% precast polyacrylamide gels (Bio-

15 Rad, Hercules, California) and transferred onto PVDF membranes 0.45µm

16 (Merk Millipore, Burlington, MA). Membranes were blocked in a mixture of Tris-

17 buffered saline and polysorbate 20 (20mM Tris-HCl pH 7.6, 150mM NaCl,

18 0.05% Tween 20) containing 5% of non-fat dry milk for 1 h at room temperature.

19 For immunoblotting have been used antibodies against HA-Tag (#3724; 1:1000,

20 Cell Signaling Technology Danvers, MA or #PA1-985; 1:1000, Thermo Fisher

21 Scientific, Waltham, MA), myc-tag (#11667149001; 1:500, Merk, Darmstadt,

22 Germany), sAC (ADCY10 PA-543049; 1:1000, Thermo Fisher Scientific,

23 Waltham, MA), TOMM20 (#sc-111415, 1:1000, Santa Cruz Biotechnology,

24 Dallas, Texas), PKA catalytic subunit (#Ab76238, 1:2000, Abcam, Cambridge,

1   UK) and Tubulin (sc-69969; 1:5000, Santa Cruz Biotechnology, Dallas, Texas) .

2   Bound primary antibodies were detected with HRP-linked antibodies (1:2000,

3   Cell Signaling Technology, Danvers, MA) and visualized by enhanced

4   chemiluminescence detection (Clarity Western ECL Substrate, Bio-Rad,

5   Hercules, California or Super Signal West Femto Maximum Sensitivity

6   Substrate, Thermo Fisher Scientific, Waltham, MA) The images have been

7   acquired on ChemiDoc Touch (Bio-Rad, Hercules, California and analysed

8   using the Image Lab software (Bio-Rad, Hercules, California)

9   **[^{35}S]GTPγS binding assay on brain homogenates**

10   Brains from 8 mice of each genotype (WT, CB_1-KO and DN22-CB_1-KI) were

11   obtained. Midbrain, cortex and hippocampus were dissected and immediately

12   stored at −70 °C until assay. For each brain region, tissue samples from each

13   genotype were pooled to obtain the enriched fractions of plasma membranes.

14   Tissue samples were homogenized using an a Teflon-glass grinder (IKA

15   Labortechnik, Satufen, Germany) at 1500 rpm (10 up-and-down strokes) in 30

16   volumes of homogenization buffer (1 mM EGTA, 3 mM $MgCl_2$, 1 mM DTT, and

17   50 mM Tris-HCl, pH 7.4) supplemented with 0.25 M sucrose. The crude

18   homogenate was centrifuged for 5 minutes at 1,000 x g at 4 ⁰C and the

19   supernatant layer was re-centrifuged for 10 minutes at 40,000 x g (4⁰C). The

20   resultant pellet (P2 fraction) was washed twice in 10 and 5 volumes of

21   homogenization buffer respectively, and re-centrifuged in similar conditions.

22   Protein content was measured according to Bradford's method using BSA as

23   standard. Samples were aliquoted in order to have a protein content of 1 mg

24   and then centrifuged in a benchtop centrifuge (EBA 12 R, Hettich Instruments,

1   Tuttlingen, Germany) at highest speed (14,000 rpm) during 15 minutes at 4 °C.

2   The supernatant layer was carefully discarded and the pellets stored at -70 °C

3   until assay. The tissue samples of the nine experimental conditions (3

4   genotypes and 3 brain regions, 1 pool for each region-genotype) were

5   processed in parallel on the same day. The day of the experiment the

6   membrane pellets were defrosted (4°C), thawed and re-suspended in 11 ml of

7   incubation buffer containing 1 mM EGTA, 3 mM $MgCl_2$, 100 mM NaCl, and 50

8   mM Tris-HCl, pH 7.4, reaching a final protein concentration of 0.09 mg/ml

9   approximately. The real final protein content was measured after the experiment

10 according to Bradford's method.

11 WIN 55,212-2 stimulated [^{35}S]GTPγS binding assays were carried out in a final

12 volume of 250 µl in 96 well plates, containing 1 mM EGTA, 3 mM $MgCl_2$, 100

13 mM NaCl, 0.2 mM DTT, 50 µM GDP, 50 mM Tris–HCl at pH 7.4 and 0.5 nM

14 [^{35}S]GTPγS. Stimulation curves were carried out by incubating increasing

15 concentrations of WIN 55,212-2 (10^{-12}-10^{-4} M; 9 concentrations by duplicate;

16 three independent experiments). The incubation was started by addition of the

17 membrane suspension (18 µg of membrane proteins per well) and was

18 performed at 30°C for 120 minutes with shaking (450 rpm). Incubation was

19 terminated by rapid filtration under vacuum (1450 FilterMate Harvester,

20 PerkinElmer) through GF/C glass fiber filters (Printed Filtermat A) pre-soaked in

21 ice-cold incubation buffer. The filters were then rinsed three times with 300 µl

22 ice-cold incubation buffer, air dried (20°C, 120 minutes), and counted for

23 radioactivity (4 minutes) by liquid scintillation spectrometry using a MicroBeta

24 TriLux counter (PerkinElmer). Non-specific binding of the radioligand was

1 defined as the remaining [^{35}S]GTPγS binding in the presence of 10 μM

2 unlabelled GTPγS, and the basal binding, as the signal in the absence of

3 agonist. The pharmacological parameters of the stimulation curves of the

4 [^{35}S]GTPγS binding, the maximal effect (Emax) and the concentration of the

5 drug that determines the half maximal effect (EC50), were obtained by non-

6 linear analysis using GraphPad Prism™ software version 5.0. The points fit to a

7 concentration-response curve (standard slope). The pharmacological

8 parameters Emax and EC50 are expressed as means ± SEM. The statistical

9 comparison of the data sets was performed in GraphPad Prism™ software

10 version 5.0, by a co-analysis of the curves.

11 **[^{35}S]GTPγS and [^{3}H]CP55,940 binding assay on brain slices**

12 [^{35}S]GTPγS (1250 Ci/mmol) and [^{3}H]CP55,940 (149 Ci/mmol) were purchased

13 from PerkinElmer (Boston MA, USA). The [^{14}C] and [^{3}H] standards were

14 supplied by American Radiolabelled Chemicals (St. Louis, MO, USA). DL-

15 dithiothreitol (DTT), guanosine-5'-diphosphate (GDP), and guanosine-5'-γ-3-

16 thiotriphosphate (GTPγS) were acquired from Sigma-Aldrich (St. Louis, MO,

17 USA). WIN 55,212-2 was purchased from Tocris Bioscience (Bristol, UK). All

18 other chemicals were obtained from standard sources and were of the highest

19 purity commercially available.

20 In order to test the ability of CB$_1$ receptor to stimulate GTPγS conversion after

21 WIN 55,212-2 administration or to bind the CP55,940 agonist, 5-6 WT and

22 DN22-*CB$_1$*-KI mice, and 1 *CB$_1$*-KO mouse as control, were sacrificed by cervical

23 dislocation and their brain rapidly frozen at -80°C. 20μm slices were cut with a

24 cryostat and mounted on superflost (Thermo Scientific, FRANCE) slides.

1   *[^{35}S]GTPγS binding assay*. Brain sections were thawed for 15 min and then

2   incubated in 50 mM Tris-HCl buffer with 3 mM MgCl$_2$, 0.2 mM EGTA, 100 mM

3   NaCl, 2 mM GDP and 1 mM DTT (pH = 7.4) for 20 min at room temperature.

4   Afterwards, the slices were incubated with 0.04 nM [^{35}S]GTPγS in absence and

5   in presence of WIN 55,212-2 μM (1 and 10 μM) for 2 h at 30°C. The non-

6   specific binding was determined with 10 μM GTPγS. Finally, the sections were

7   washed twice in 50 mM Tris-HCl (pH =7.4) for 15 min at 4°C, dried and exposed

8   to a Kodak Biomax MR film with ^{14}C standards. The films were scanned and

9   quantified by transforming the optical densities into nCi/mg using the ^{14}C

10   standards (NIH-IMAGE, Bethesda, MA, USA). The background and the non-

11   specific densities were subtracted. The percentages of stimulation were

12   calculated from the basal and agonist-stimulated [^{35}S]GTPγS binding densities

13   according to the formula (stimulated x 100/basal) - 100.

14   *[^{3}H]CP55,940 binding assay*. Tissue sections were dried and incubated in 50

15   mM Tris-HCl buffer containing 1% of BSA (pH = 7.4) for 30 min at room

16   temperature. Later, the brain sections were incubated again in the same buffer

17   supplemented with 3 nM [^{3}H]CP55,940 for 2h at 37°C. Non-specific binding was

18   determined with 10 μM WIN 55,212-2. Finally, sections were washed in ice-cold

19   50 mM Tris-HCl buffer supplemented with 1% BSA followed by dipping in

20   distilled water at 4°C. After drying, the brain slides were exposed to a radiation

21   sensitive film for 21 days at 4°C together with tritium standards. The films were

22   scanned and quantified by transforming the optical densities into nCi/mg using

23   the tritium standards (NIH-IMAGE, Bethesda, MA, USA). The background and

24   the non-specific densities were subtracted to determine the specific binding.

Behavioral tests

Wire hang test. Wild type and DN22-CB_1-KI mice were tested for their muscular strength in the wire hang test(Redon et al., 2020). All tests were conducted during the dark phase of the cycle under dim red light. Each cage, housing one mouse, was placed on a bench in a room adjacent to the one housing the mice. Thereafter, each mouse was removed from its cage, placed on the cage grid, the latter being then slowly inverted as to be suspended 90 cm above a big cage filled with polystyrene beads. The latency to fall was then recorded.

Basal locomotion. The basal locomotor activity of WT and DN22-CB_1-KI mice was measure during seven days using the TSE PhenoMaster system (TSE Systems GmbH). Mice were placed individually in a plexiglass cage [45cm (length) X 34cm (width) X 20cm (height)] surrounded with the ActiMot module containing IR light beams recognizing locomotor activity. Food and water were available *ad libitum.*

Catalepsy, locomotion and antinociception. AM251 and Hemopressin were bilaterally injected into the SNr in a volume of 0.5 µl per side. Immediately after, THC (10 mg/kg) was injected i.p. Mice were tested, 30 min post-injections, successively for catalepsy, locomotion and antinociception. Locomotor activity was tested by placing the mouse in a novel environment and the number of squares crossed was counted for 5 minutes. For seek of clarity, given the fact that striatonigral CB_1 receptor deletion did not affect the hypo-locomotor effects of THC (**Figure S1B and S1E**), we did not show results for this behavioral paradigm for the other experimental sets. The catalepsy was determined by the time of immobility on a bar. To this aim, mice were positioned in a new plastic

1   cage (identical to their home cage) without bedding with on a horizontal

2   cylindrical bar (0.7cm Diameter) placed at 4.5 cm high with their forepaws

3   gripping and its hind paws in the plastic box. The time spent in its initial position

4   on the bar was scored for two minutes. Immediately after, mice were placed in

5   a Hot Plate (BIOSEB) to measure antinociception. The plate was pre-heated at

6   52°. The escape latency, defined as the time until the mice showed signs of

7   discomfort (paw licking, jumping), was recorded. All equipment was cleaned

8   with ethanol 25% and dried with paper towels between all the trials. For AAVs

9   injected mice the procedure was identical but mice were tested 5 weeks after

10 viral injections.

11 **Immuno-electron microscopy**

12 The experiments were performed as described previously(Puente, 2019). CB_1-

13 KO, DN22-CB_1-KI, and respective WT littermates mice (n = 3 per genotype)

14 were deeply anesthetized by intraperitoneal injection of ketamine/xylazine

15 (80/10 mg/kg body weight i.p.) and were transcardially perfused at room

16 temperature (RT, 20-25°C) with phosphate buffered saline (0.1 M PBS, pH 7.4)

17 for 20 s, followed by the fixative solution made up of 4% formaldehyde (freshly

18 depolymerized from paraformaldehyde), 0.2% picric acid, and 0.1%

19 glutaraldehyde in phosphate buffer (0.1 M PB, pH 7.4) for 10-15 min. Once the

20 animals were perfused, the brains were numbered by a different experimenter

21 to conduct the protocol blindly. Then, brains were removed from the skull and

22 post-fixed in the fixative solution for approximately 1 week at 4°C. Afterwards,

23 brains were stored at 4°C in 1:10 diluted fixative solution until used.

1   *Pre-embedding silver-intensified immunogold method.* The method applied was

2   already described(Puente, 2019). Coronal midbrain vibratome sections

3   containing the substantia nigra pars reticulata were cut at 50 μm and collected

4   in 0.1 M PB (pH 7.4) with 0.1% sodium azide at RT. Sections were

5   preincubated in a blocking solution of 10% bovine serum albumin (BSA), 0.1%

6   sodium azide, and 0.02% saponin prepared in Tris-HCl buffered saline (TBS

7   1X, pH 7.4) for 30 min at RT. Then, sections were incubated with a primary goat

8   anti-CB_1 antibody binding to a 31 amino acids sequence of the C-terminus (CB_1

9   C-ter[31]; 2 µg/ml; Cat. N.: CB_1-Go-Af450-1; Frontier Institute; Japan) in the

10 blocking solution but with 0.004% saponin on a shaker for 1 day at RT. After

11 several washes in 1% BSA/TBS, tissue sections were incubated in a secondary

12 anti-goat 1.4 nm gold-labeled Immunoglobulin-G antibody (Fab' fragment,

13 1:100, Nanoprobes Inc.) in 1% BSA/TBS with 0.004% saponin on a shaker for 4

14 h at RT. Thereafter, the tissue was washed in 1% BSA/TBS overnight at 4°C

15 and post-fixed in 1% glutaraldehyde in TBS for 10 min at RT. Following washes

16 in double distilled water, gold particles were silver-intensified with a HQ Silver

17 kit (Nanoprobes Inc., Yaphank, NY, USA) for about 12 min in the dark and then

18 washed in 0.1 M PB (pH 7.4). Stained sections were osmicated (1% osmium

19 tetroxide, OsO_4, in 0.1 M PB pH 7.4, 20 min), dehydrated in graded alcohols to

20 propylene oxide, and plastic-embedded flat in Epon 812. To localize the region

21 of interest, immunolabeled resin-embedded vibratome sections were first

22 visualized by light microscopy to select the portion of the SN and to ensure that

23 the slices have the appropriate antibody labeling. Then, semithin (700 nm)

24 sections are mainly extracted to remove the resin and reach the tissue.

25 Afterwards, we started to collect ultrathin sections of 50 nm on mesh nickel

41

1 grids, stained with 2.5% lead citrate for 20 min, and examined in a Philips

2 EM208S electron microscope. Photographs are always taken in the area of

3 interest and close to the resin; in this way we know that we are a few

4 nanometers from the surface, and that the immunelabeling is complete.

5 Furthermore, we photographed in a range of 0 to at most 950 nm from the

6 surface, because the first 5 ultrathin sections of 50 nm are collected. Tissue

7 preparations were photographed by using a digital camera coupled to the

8 electron microscope. Figure compositions were made at 300 dots per inch (dpi).

9 Labeling and minor adjustments in contrast and brightness were made using

10 Adobe Photoshop (CS, Adobe Systems, San Jose, CA, USA).

11 *Semi-quantification of mtCB$_1$ receptor immunostaining using immunogold*

12 *method.* Analyses were carried out according to previous publications

13 (Gutierrez-Rodriguez et al., 2018; Hebert-Chatelain et al., 2016; Puente et al.,

14 2019). 2-3 of 50 µm-thick sections containing the substantia nigra pars

15 reticulata and hippocampus from each animal genotype (n=3 each) showing

16 good and reproducible silver-intensified gold particles were cut at 50 nm. To

17 minimize differences between groups, all sections were processed

18 simultaneously. Three separate experiments were performed for each animal.

19 Electron micrographs were taken from grids with similar labeling intensity

20 indicating that selected areas were at the same depth. To avoid false negatives,

21 only ultrathin sections in the first 1.5 µm from the surface were examined. Total

22 CB$_1$ receptor labeling and total CB$_1$ particles in plasma and mitochondrial

23 membranes were counted per area. The proportion of CB$_1$ receptor-positive

24 mitochondria was calculated for each mouse counting only particles (at least

25 one) on mitochondrial membrane segments far away from other membranes

42

1 (distance ≥ 80 nm). Image-J (version 1.36) was used to measure the distance.

2 Graphs and statistical analyses were performed using GraphPad software

3 (version 5.0).

4 **_In vitro_ characterization of mt-sAC and PKA mutants**

5 _Confocal Microscopy Imaging._ HeLa cells seeded on 12-mm round glass

6 coverslips and transfected as indicated, were placed on the stage of the

7 Olympus FV3000 confocal fluorescence microscope (Tokyo, Japan) and

8 imaged using a 60X oil objective (UPLAN 60× oil, 1.35 NA, Olympus), and

9 appropriate excitation laser and filters. For each experiment, 15 cells were

10 randomly selected and analyzed. Stacks of 30 images separated by 0.2 μm

11 along the Z axis were acquired. Three-dimensional reconstruction and volume

12 rendering of the stacks were carried out with the appropriate plug-in of ImageJ

13 (NIH, Bethesda, MD, USA). Pearson's correlation coefficient for TOM20

14 fluorescence colocalization with Myc or HA, was calculated with the

15 Colocalization threshold tool of ImageJ.

16 _Trypsin Sensitivity Assay._ The trypsin sensitivity assay was carried out as

17 described previously (Choo, 2004) with minor modifications. Isolation of

18 mitochondrial fractions was performed as described previously (Guedouari et

19 al., 2017). Briefly, HeLa cells were harvested and resuspended in mitochondrial

20 isolation buffer (250 mM sucrose, 1 mM EDTA, 5 mM HEPES, pH 7.4)

21 supplemented with 1% protease inhibitor cocktail (Bioshop, ON, Canada), 2 mM

22 sodium orthovanadate and 1 mM sodium fluoride. Cells were lysed with 15

23 strokes using a 25-gauge syringe on ice and centrifuged at 1500× g for 5 min (4

24 °C). The resulting supernatant was centrifuged at 12,500× g for 10 min (4 °C).

25 pellet was resuspended in the mitochondrial buffer and a cycle of centrifugation

1 at 1500× g and 12,500× g was repeated. The final pellet was considered as the

2 mitochondria-enriched fraction. Protein concentration was determined by

3 Bradford assay (Bradford, 1976). Isolated mitochondria were suspended in

4 mitochondrial isolation buffer and incubated at 37 °C for 10 min in presence or

5 absence of trypsin (0.5%) and triton X-100 (1%). Reaction was stopped by the

6 addition of 1% of the protease inhibitor cocktail. Mitochondria were then

7 centrifuged at 12,500× g at 4 °C for 10 min. The pellets were processed for

8 SDS-PAGE and subsequent western blotting.

9 **Sniffer cells detection of Substance-P release**

10 cDNA for human NK_1 was purchased from the cDNA resource center

11 (www.cdna.org). NK_1-mCherry plasmid was created by cloning the mCherry

12 coding sequence in frame with the C-terminus of NK_1 with its stop codon

13 removed by PCR.

14 *System validation in vitro*. NK_1-mCherry was co-transfected with GCaMP6s

15 (Addgene) into HEK293 cells (Cedarlane) seeded on coverslips using

16 Lipofectamine 2000 (Invitrogen). 24-48 hours later, coverslips were transferred

17 to a perfusion chamber containing EBS (in mM: NaCl 140, KCl 5.4, $CaCl_2$ 1.3,

18 HEPES 10, glucose 33, pH 7.35) and allowed to equilibrate for 10-15 minutes at

19 room temperature with a flow rate of ~1ml/min. Baseline GCaMP6s

20 fluorescence was recorded for 60 seconds. Then Substance-P (Tocris) was

21 added to the chamber using a micropipette to achieve final concentrations of

22 10^{-11}M-10^{-6}M. 16-bit Images were collected at 1Hz on an Olympus BX-61

23 microscope with a 20X water immersion objective and a Hamamatsu ORCA-

24 Flash4 CCD camera. Using ImageJ, the change in fluorescence normalized to

25 baseline fluorescence (ΔF/F0) was calculated following background subtraction

by binning the 30 frames prior to Substance-P stimulation (F0) and 30 frames surrounding the peak response following Substance-P stimulation. The perfusion chamber was washed with 50mL of EBS over 15 minutes between coverslips. When necessary, rundown was corrected using the Bleach Correction algorithm in ImageJ and the occasional flicker of the microscope bulb was corrected manually.

Substance-P and WIN 55,212-2 effect in vitro. HEK cells were seeded on glass coverslips coated with poly-lysine and transfected with plasmid DNA for NK_1-mCherry and GCaMP6s or Empty vector and GCaMP6s with PEI (**Figure S1I**). Cells were imaged 24-48 hrs after transfection on epifluorescence mode with an inverted spinning-disk microscope equipped with 40X objective (NA 1.4), a multi-LED illumination system and a CDD camera. Coverslips were mounted on a open chamber and superfused with a buffer solution of (in mM): 112 NaCl, 5 KCl, 24 NaHCO3, 10 HEPES, 1.25 $CaCl_2$, 1.25 $MgCl_2$, 5 glucose, bubbled with air/5% CO_2 (pH 7.4) at 36°C. For experiments on cells expressing NK_1-mCherry/ GCaMP6s, cells expressing NK_1 were first selected by 570 nm illumination and emission collection at 617/36 nm before starting Ca^{2+} imaging. Cells expressing GCaMP6s were excited at 490 nm for 0.05-0.1 s and emission collected at 524/16 nm. Data was background corrected and represented as normalized fluorescence. Substance-P and WIN55.212-2 were applied for 1 minute and recording were performed for the next 5 minutes (**Figure S1L**).

Substance-P release from striatonigral terminals. Sagittal sections containing SNr were prepared from 6 to 12 weeks-old mice. For electrical stimulation, naive CB_1-KO, DN22-CB_1-KI, and respective WT littermates were used. For optogenetic activation of striatonigral terminals 6 weeks-old D1-Cre mice were

1   used to target striatal neurons with injection of a rAAV-hSyn-DIO-ChrimsonR-

2   tdTomato into the dorsal Striatum (in mm relative to bregma: AP=+0.8, L=±2.0,

3   DV=-2.7) 6 weeks before experiments.

4   Mice were first sedated by inhaling isoflurane (4%) for approximately 30 s and

5   then deeply anesthetized with a mixture of ketamine and xylazine (100 and 20

6   mg/kg, i.p., respectively). After the disappearance of the reflexes, a thoracotomy

7   was performed to allow transcardial perfusion of a saturated (95% O_2/5% CO_2)

8   ice-cold solution containing 250 mM sucrose, 10 mM $MgSO_4 \cdot 7H_2O$, 2.5 mM

9   KCl, 1.25 mM $NaH_2PO_4 \cdot H_2O$, 0.5 mM $CaCl_2 \cdot H_2O$, 1.3 mM $MgCl_2$, 26 mM

10   $NaHCO_3$ and 10 mM D-glucose. After decapitation, each brain was quickly

11   removed and cut into sagittal slices (300 µm) using a vibratome (VT-1200S;

12   Leica Microsystems, Germany). The slices were then incubated at 34°C for 10

13   min in a standard artificial cerebrospinal fluid (ACSF) saturated by bubbling

14   95% O_2/5% CO_2 and containing 126 mM NaCl, 2.5 mM KCl, 1.25 mM

15   $NaH_2PO_4 \cdot H_2O$, 2 mM $CaCl_2 \cdot H_2O$, 2 mM $MgSO_4 \cdot 7H_2O$, 26 mM $NaHCO_3$ and 10

16   mM D-glucose, supplemented with 5 µM glutathion and 1 mM sodium pyruvate.

17   Transfected HEK cells (*see above*) re-suspended in ACSF were gently

18   deposited over the slices that were placed in a small petri-dish. Slices were

19   allowed to rest for 2h to allow the sniffer cells to attach to the tissue before

20   starting the recording. Slices were then transferred in a recording chamber

21   under an upright microscope (Ni-E, Nikon Instruments). For electrical

22   stimulation experiments, a bipolar stimulating electrode was placed in proximity

23   of *capsula interna* and trains of electrical stimulation were applied. For

24   optogentic activation, an optic fiber was placed above the SNr and trains of

25   570nM light pulses (5s 20 Hz) were applied. The presence of the receptor and

the fluorescence of GCaMP6s in HEK cells were observed and measured with an infrared differential interference system using a 60x immersion lens. The image detection was done with a camera (Zyla, Andor technology). GCaMP6s was excited using 470 nm light supplied by a LED device (Lumencor). Images were collected at 10 Hz. Image stacks were imported into Image J software where changes in fluorescence in HEK cell were measured over time. Imaged were post-processed to calculate ΔF. Regions of interest (ROI) corresponded to HEK cell visually identifiable and expressing both GCaMP6s and Substance-P Receptor were delimited. The fluorescence time course F of each ROI was measuring by averaging all pixels within the ROI. Background fluorescence was subtracted from all values. Fluorescence at various time points was expressed relative to baseline. Stimulus-induced changes in fluorescence were calculated from the maximum value observed during a 30 s period following the onset of the response and expressed relative to baseline (average of values collected 10 s before the electrical stimulation or 3 s before red-light stimulation). Negative controls on brain slices were performed either by using HEK cells transfected only with GCaMP6s and not NK1-R (*see above*) or by GCaMP6s/NK1-R expressing HEK cells in presence of the selective Substance-P Receptor blocker CP122721. Control experiments for whole-cell voltage-clamp recordings of oIPSCs were performed as described in the next session.

Electrophysiology

Optogenetic activation of striatonigral terminals. Male DN22-CB_1-KI mice, CB_1-KO mice and their WT littermates were used to target striatal neurons with injection of a AAV2-hSyn-ChR2(H134R)-mCherry into the dorsal Striatum (in

mm relative to bregma: AP=+0.8, L=±2.0, DV=-2.7) 8-9 weeks before electrophysiological recordings. Mice were sedated with isoflurane, deeply anesthetized with ketamine/xylazine (75/10 mg/Kg) and perfused transcardially with ice-cold modified artificial cerebrospinal fluid (ACSF), equilibrated with 95% O_2 and 5% CO_2, and containing (in mM): 230 sucrose, 26 $NaHCO_3$, 2.5 KCl, 1.25 NaH_2PO_4, 0.5 $CaCl_2$, 10 $MgSO_4$ and 10 glucose. Brains were rapidly removed and sectioned into 300 µm-thick parasagittal slices with a vibrating blade microtome (VT1200S; Leica Microsystems, Germany). Slices containing the SNr were then left to equilibrate for 1 h (at 35°C) in ACSF of the following composition (in mM except otherwise specified): 126 NaCl, 26 $NaHCO_3$, 2.5 KCl, 1.25 NaH_2PO_4, 2 $CaCl_2$, 2 $MgSO_4$, 10 glucose, 1 sodium pyruvate and 4.9µM L-gluthathione reduced (gassed with 95% O_2 and 5% CO_2). Single slices were transferred to a recording chamber, perfused continuously with modified oxygenated ACSF at 32-34°C containing (in mM): 126 NaCl, 26 $NaHCO_3$, 3 KCl, 1.25 NaH_2PO_4, 1.6 $CaCl_2$, 1.5 $MgSO_4$, 10 glucose, and visualized using infrared gradient contrast video microscopy and a 60X water-immersion objective (Fluor 60X/1.00 W, Nikon). Recordings from individual SNr neurons were made using pipettes (impedance, 6-8 MΩ) prepared from borosilicate glass capillaries (G150-4; Warner Instruments, Hamden, CT, USA) with a micropipette puller (P-97; Sutter Instruments, Novato, CA, USA). For whole-cell voltage-clamp recordings, pipettes were filled with (in mM): 130 K-gluconate, 6.6 Na-gluconate, 1 $MgCl_2.6H_2O$, 10 HEPES, 5 QX-314, 0.1 Na_4EGTA, 0.4 Na_3GTP, 2 $Mg_{1.5}ATP$ and 5.4 biocytin. The pipette solution had a pH of 7.2 and an osmolarity of 292 mOsm. Recordings were obtained using a Multiclamp 700B amplifier and Digidata 1440 digitizer controlled by Clampex 10.3

1   (Molecular Devices, Sunnyvale, CA, USA). Signals were low-pass filtered at 4

2   kHz and sampled at 20 kHz. Whole-cell voltage clamp recordings with

3   Kgluconate-filled electrodes were corrected for a junction potential of 13 mV. In

4   voltage clamp experiments, series resistance was monitored by a step of -5 mV

5   at the end of each recording. Optogenetic activation of SNr terminals was

6   performed *via* optic fiber as previously described (Froux et al., 2018)

7   After 5 minutes baseline, CB_1 receptor was activated with 5 µM WIN 55,212-2

8   dissolved in DMSO. This concentration has been previously showed to reduce

9   hippocampal EPSCs in a CB_1 dependent manner(Hebert-Chatelain et al.,

10 2016). The glutamatergic synaptic transmission was not blocked for all

11 electrophysiological experiments. Levels of drug-induced depression in

12 response to WIN 55,212-2 are reported as averaged IPSC amplitudes for 5 min

13 just before bath application compared with averaged IPSC amplitudes during

14 the 15-min period after the application. Data were discarded when the series

15 resistance varied by >20%. After electrophysiological recordings, slices were

16 fixed overnight in a solution of paraformaldehyde at 4% and maintained in PBS-

17 azide at 0.3% at 4°C until histological processing for mCherry visualization or

18 TH/biocytin immunostaining(Chazalon et al., 2018).

19 *Hippocampal depolarization-induced suppression of inhibition.* Male DN22-CB_1-

20 KI mice and their WT littermates were sacrificed by dislocation and the brain

21 was immediately immersed in ice-cold oxygenated cutting solution containing in

22 mM: 180 Sucrose, 26 $NaHCO_3$, 12 $MgSO_4$, 11 Glucose, 2.5 KCl, 1.25

23 NaH_2PO_4, and 0.2 $CaCl_2$, oxygenated with 95% O_2-5% CO_2 ≈300mOsm.

24 Parasagittal hippocampal slices (300µm thick) were obtained using a vibratome

25 (VT1200S, Leica, Germany) and transferred for 30min into a 34°C bath of

1 oxygenated ACSF containing in mM: 123 NaCl, 26 NaHCO$_3$, 11 Glucose, 2.5

2 KCl, 2.5 CaCl$_2$, 1.3 MgCl$_2$, 1.25 NaH$_2$PO$_4$ ≈305 mOsm. After a minimum of 1h

3 recovery at room temperature (22-25°C), slices were transferred to a recording

4 chamber in ACSF at 32°C. Whole-cell recordings of IPSCs were made using a

5 MultiClamp 700B amplifier (Molecular devices, UK) in CA1 pyramidal neurons

6 voltage clamped at −70mV with a pipette (3-5 MΩ) containing in mM: 130 KCl,

7 10 HEPES, 1 EGTA, 2 MgCl$_2$, 0.3 CaCl$_2$, 7 Phosphocreatin, 3 Mg-ATP, 0.3 Na-

8 GTP; pH = 7.2; 290mOsm. Evoked IPSCs were performed by a monopolar

9 stimulating patch pipette filled with ACSF in stratum radiatum in presence of

10 NMDA and AMPA/Kainate receptor antagonists (50µM D-APV and 10µM

11 NBQX).

12 DSIs were performed by depolarizing pyramidal neurons from −70mV to 0mV

13 for 3 s. DSIs' magnitude were measured as the average of 3 DSIs with 2min

14 apart and represented the percentage of change between the mean of the 5

15 consecutive IPSCs preceding the depolarization and the first three IPSCs

16 following the depolarization, with IPSCs evoked every 3 s. Currents were

17 filtered at 4kHz by a Digidata 1440A (Molecular devices, UK) and were

18 analyzed using either Clampfit software (pClamp10).

19 **Data collection and statistical analyses**

20 No statistical methods were used to pre-determine sample sizes, but they are

21 similar to those reported in previous publications. Data collection and analysis

22 were performed blind to the conditions of the experiment. All mice were

23 assigned randomly to the different experimental conditions.

1   All graphs and statistical analyses were performed using GraphPad software

2   (version 5.0, 6.0 or 8.0). Results were expressed as means of independent data

3   points ± s.e.m. Behavioral data where checked for normality distribution with the

4   D'Agostino&Pearson test. When all groups of an experiment passed the

5   normality test, ANOVA (One-way or Two-way, where appropriate) analysis was

6   performed and when interaction was significant Tukey's post hoc analysis was

7   used. When the normality was rejected, non-parametric One-way ANOVA

8   (Kruskal-Wallis) was used (**Table S2 and S3**). Biochemical, anatomical,

9   imaging and electrophysiological data were analyzed using Student's *t*-test

10   (unpaired or paired, where appropriate) or Wilcoxon test as appropriate (**Table**

11   **S2 and S3**). Post hoc significances were expressed as follow: * p<0.05, **

12   p<0.01, *** p<0.001.

13

FIGURE LEGENDS

Figure 1. Striatonigral CB$_1$ receptors mediate catalepsy and antinociception.

(**A and B**) Effects of correct "hit" or misplaced "no-hit" intra-SNr administration of the cell permeable CB$_1$ antagonist AM251 on the (**A**) cataleptic, and (**B**) antinociceptive THC effect (10mg/kg i.p.) respect to vehicle treated mice.

(C) Representative micrograph (left) and relative quantification (right) of CB$_1$ immunoreactivity in the GPe (white bars) and the SNr (black bars) of mice with striatopallidal (ST-GP-*CB$_1$*-KO) or striatonigral (ST-SN-*CB$_1$*-KO) CB$_1$ receptor deletion compared to control littermates. Target regions are indicated by yellow dotted lines.

 (D) Cataleptic and **(E)** antinociceptive effects of THC (10mg/kg i.p.) in mice with striatopallidal (ST-GP-*CB$_1$*-KO) or striatonigral (ST-SN-*CB$_1$*-KO) CB$_1$ receptor deletion compared to control littermates.

(**F and G**) Effects of intra-SNr administration of the cell impermeable CB$_1$ antagonist Hemopressin (Hp) on the **(F)** cataleptic, and **(G)** antinociceptive effect of systemic THC (10mg/kg i.p.) respect to vehicle treated mice.

(H and I) Effects of intra-SNr administration of the NK$_1$ receptor agonist GR73632 on the (**H**) cataleptic, and **(I)** antinociceptive effect of THC (10mg/kg i.p.) respect to vehicle treated mice.

(J) Schematic representation of the Substance-P sniffer strategy, and representative picture of sniffers cells [HEK cell expressing NK$_1$ receptor

1   (NK$_1$R) (red) and GCaMP6 (green)] deposited over slices (IR). Stim: electrical

2   stimulation, STR: striatum, SNr: Substantia nigra pars reticulata, GPe: external

3   globus pallidus. Scale bars: 50 μm.

4   (**K)** Left: Representative GCaMP6 fluorescence in the SNr before and after

5   electrical stimulation, in presence of vehicle or WIN (5µM). Middle: traces of

6   GCaMP6 fluorescence variation (ΔF/F0) from sniffer cells overlying the area

7   shown in **(K)** (right panel, white square) in the absence (Vehicle) and in the

8   presence of WIN when electrical stimulation (gray bars) of the striatonigral

9   pathway is applied in both WT and *CB$_1$*-KO littermates. Plots are from the same

10   cells in both conditions. Right: summary graphs comparing ΔF induced by

11   electrical stimulation in all sniffer cells responding and imaged over the SNr in

12   Vehicle and WIN conditions, comparing WT vs *CB$_1$*-KO littermates.

13   **(L)** Schematic representation of the Substance-P sniffer strategy coupled to

14   optogenetic stimulation of striatonigral terminals. SNr: Substantia nigra pars

15   reticulata, GPe: external globus pallidus.

16   **(M)** Left: traces of GCaMP6 fluorescence variation (ΔF/F0) from sniffer cells

17   overlying the SNr in the absence (Vehicle) and in the presence of WIN when

18   light stimulation (red bars) of the striatonigral pathway is applied. Plots are from

19   the same cells in both conditions. Right: summary graphs comparing ΔF

20   induced by light stimulation in all sniffer cells responding and imaged over the

21   SNr in Vehicle and WIN conditions.

22

23

1 **Figure 2. CB$_1$ receptor subcellular localization in the SNr.**

2 **(A - E)** Immunogold detection of CB$_1$ receptor by electron microscopy in WT

3 and *CB$_1$*-KO mice in SNr. White arrows, plasma membrane gold particles; pink

4 arrows, mitochondrial gold particles; scale bar: 500 nm. Den, dendrites; ter,

5 synaptic terminal, m, mitochondrion; red arrowheads, synapses. Relative

6 quantifications of total CB$_1$ receptor labeling (**B**), plasma membrane CB$_1$

7 (pmCB$_1$) receptor labeling **(C)**, mitochondrial-associated CB$_1$ (mtCB$_1$) receptor

8 labeling **(D)** and proportion of CB$_1$ receptor-positive mitochondria **(E)**.

9 **(F - J)** Immunogold detection of CB$_1$ receptor by electron microscopy in WT and

10 DN22-*CB$_1$*-KI mice in SNr. White arrows, plasma membrane gold particles; pink

11 arrows, mitochondrial gold particles; scale bar: 500 nm. Den, dendrites; ter,

12 synaptic terminal, m, mitochondrion; red arrowheads, synapses. Relative

13 quantifications of total CB$_1$ receptor labeling (**G**), plasma membrane CB$_1$

14 (pmCB$_1$) receptor labeling **(H)**, mitochondrial-associated CB$_1$ (mtCB$_1$) receptor

15 labeling **(I)** and proportion of CB$_1$ receptor-positive mitochondria **(J)**.

16 **(K)** Concentration–response curves of the effect of WIN on [^{35}S]GTPγS binding

17 in membranes isolated from cortex, hippocampus and midbrain of WT, *CB$_1$*-KO

18 and DN22-*CB$_1$*-KI mice.

19 **(L)** The effect of WIN (1µM) on mitochondrial respiration (oxygen consumption

20 rate, OCR) in SNr homogenates from WT, *CB$_1$*-KO, and DN22-*CB$_1$*-KI mice.

21 Data are expressed as percentage of vehicle values.

22

54

1 **Figure 3. Striatonigral mtCB$_1$ receptor functions.**

2 **(A)** Representative picture of the striatonigral pathway targeted with optogenetic

3 tools. STR, striatum; GPe, external globus pallidus; STN, subthalamic nucleus;

4 TH, thalamus; HP, hippocampus; SNr substantia nigra pars reticulata. Scale bar

5 500µM.

6 **(B)** Representative post-hoc characterization of the analyzed cells (white arrow)

7 by immunofluorescence for biocytin, mCherry (ChR2) and thyroxine-

8 hydroxylase (TH). Scale bar: 50µM.

9 (**C**) Representative traces of light evoked inhibitory post-synaptic currents

10 (oIPSCs) under control condition and in presence of the GABA$_A$ receptor

11 blocker Gabazine (GBZ) with its corresponding time-course effect.

12 **(D)** Time course effect of WIN (5 µM) on striatonigral oIPSCs in slices derived

13 from WT, *CB$_1$*-KO and DN22-*CB$_1$*-KI mice.

14 (**E)** Plots of normalized oIPSCs with representative traces before and after WIN

15 treatment and summary of the average change of oIPSCs relative to baseline.

16 **(F)** Cataleptic, and **(G)** antinociceptive effect of systemic THC (10mg/kg i.p.) or

17 WIN (3mg/kg i.p.), respect to vehicle in WT and DN22-*CB$_1$*-KI mice

18

19

1 **Figure 4. Striatonigral mtCB$_1$ receptor signaling.**

2 **(A)** Schematic representation of the CB$_1$ or DN22-CB$_1$ rescue-approach in D$_1$-

3 *CB$_1$*-KO mice. STR, striatum; SNr, substantia nigra pars reticulata; mtCB$_1$,

4 mitochondrial CB$_1$ receptor; pmCB$_1$, plasma membrane CB$_1$ receptor.

5 **(B)** Representative immunofluorescence pictures of CB$_1$ or DN22-CB$_1$ rescue in

6 the SNr of D$_1$-*CB$_1$*-KO mice. Green, CB$_1$ positive signal; Blue, DAPI nuclear

7 counterstaining. Scale bar 250μm.

8 **(C)** Relative quantification of CB$_1$ receptor immunofluorescence D$_1$-*CB$_1$*-KO

9 mice after CB$_1$ or DN22-CB$_1$ rescue in the SNr.

10 **(D)** Effect of WIN (1μM) on mitochondrial respiration (oxygen consumption rate,

11 OCR) in SN homogenates form WT, D$_1$-*CB$_1$*-KO control mice, and CB$_1$ or

12 DN22-CB$_1$ rescued in the striatonigral circuit (*see above **A and B***).

13 (**E**) Cataleptic effect of THC (10mg/kg i.p.) in WT, D$_1$-*CB$_1$*-KO control mice, and

14 CB$_1$ or DN22-CB$_1$ rescued in the striatonigral circuit (*see above **A and B***).

15 **(F)** Effect of WIN (1μM) on mitochondrial respiration (oxygen consumption rate,

16 OCR) in SN homogenates pre-treated with vehicle or the sAC blocker KH7

17 (5μM).

18 (**G and H)** Effects of intra-SNr administration of sAC blocker KH7 (2μg) on the

19 **(G)** cataleptic, and **(H)** antinociceptive effect of systemic THC (10mg/kg i.p.)

20 respect to vehicle treated mice.

1 **(I)** Effect of WIN (1µM) on mitochondrial respiration (oxygen consumption rate,

2 OCR) in SN homogenates form D_1-Cre mice injected in the striatum with control

3 (Ctr) virus or Cre-dependent mt-sAC expressing virus.

4 **(J)** Cataleptic, and **(K)** antinociceptive effects of systemic THC (10mg/kg i.p.)

5 respect to vehicle in D_1-Cre mice injected with either control (Ctr) or Cre-

6 dependent mt-sAC expressing virus in the striatum.

7 **(L)** Cataleptic, and **(M)** antinociceptive effect of systemic THC (10mg/kg i.p.)

8 respect to vehicle in D_1-Cre mice injected with either control (Ctr) or Cre-

9 dependent PKA-CA or MLS-PKA-CA expressing virus in the striatum.

10 **(N)** Effect of WIN (1µm) on mitochondrial respiration (oxygen consumption rate,

11 OCR) in SN homogenates from D_1-Cre mice injected in the striatum with control

12 virus or Cre-dependent PKA-CA or MLS-PKA-CA vectors.

13

14

15

16

17

18

19

20

SUPPLEMENTARY FIGURE LEGENDS

Figure S1 (related to main Figure 1). Cannabinoid-induced antinociception, but not catalepsy, relies on activation of striatonigral pmCB$_1$ and regulation of Substance-P/NK$_1$ receptor activity.

(A) SNr correct (hit) and misplaced (no-hit) cannula placements verified by infusion of skyblue toluidine solution followed by brain slicing and neutral red counterstaining. Representative histological analysis (top) and schematic representations (bottom, "hit" green dots, "no-hit" red dots) of the injection sites in the SNr.

(B) Effects of correct "hit" and misplaced "no-hit" intra-SNr administration of the cell permeable CB$_1$ antagonist AM251 on the hypolocomotor effect of systemic THC (10mg/kg i.p.) respect to vehicle treated mice.

(C) Schematic for striatonigral or striatopallidal CB$_1$ receptor deletion and representative pictures of viral injection sites. Green signal, striatal (STR) expression of AAV-FRT-iCre-EGFP. Blue signal, AAV-retro-FLP-BLFP or AAV-retro-BLFP expression in the globus pallidus (GPe) or in the substantia nigra reticulata (SNr).

(D) Representative micrograph (left) and relative quantification (right) of CB$_1$/D$_1$ and CB$_1$/D$_2$ co-expressing cells in the striatum of mice with striatopallidal (ST-GP-*CB$_1$*-KO) or striatonigral (ST-SN-*CB$_1$*-KO) CB$_1$ receptor deletion compared to control littermates. ec: external capsule. ns: non–statistically different. Scale bar, 50µm.

(E) Hypolocomotor effect of systemic THC (10mg/kg i.p.) respect to vehicle in mice with striatopallidal (ST-GP-CB_1-KO) or striatonigral (ST-SN-CB_1-KO) CB_1 receptor deletion compared to control littermates.

(F-G) Effects of i.p. administration of the NK_1 receptor agonist GR73632 (75 μg/kg) on the cataleptic **(F)** and antinociceptive **(G)** effects of systemic THC (10mg/kg i.p.) respect to vehicle treated mice.

(H) Left: Schematics of the Substance-P (SP) "sniffer cell" system. Co-expression of human NK_1 receptor (hNK_1R) and GCaMP6s in HEK293T cells facilitates detection of SP-induced calcium increases reflected by increased GCaMP6s fluorescence. Center: fluorescence micrographs of representative SP "sniffer cells" co-expressing hNK_1R-mCherry and GCaMP6s, and line-scan fluorescence quantification indicating membrane localization of hNK_1R. Right: representative fluorescence micrographs and kinetic trace of SP "sniffer cells" at baseline (time=0s) and following stimulation with 10nM SP (time=180s) added to the perfusion chamber following a 60s baseline recording. Dose response to SP in the same settings (bottom right) quantified as the change in GCaMP6s fluorescence normalized to baseline fluorescence (ΔF/F0) with increasing doses of SP. The EC50 for "sniffer cells" to SP was 5.088nM.

(I) GCaMP6 response to different doses of SP in presence of NK_1R or in its absence, indicating the specificity of the "sniffer cell" response.

(J) Left: traces of GCaMP6 fluorescence variation (ΔF/F0) from sniffer cells expressing only GCaMP6 or both GCaMP6/NK_1R in the absence (Vehicle) and in the presence of the NK_1R blocker CP122721 (CP) when electrical stimulation (gray bars) of the striatonigral pathway is applied. Right: summary bar graphs

1   comparing means ± SE values of ΔF induced by electrical stimulation in all

2   sniffer cells responding and imaged over the SNr in Vehicle and CP conditions

3   **(K)** GCaMP6 fluorescence changes (ΔF) after electrical stimulation in control

4   condition, after vehicle and 5µM WIN on the same cells.

5   **(L)** Induction of calcium increase by SP in presence of 5µM WIN *in vitro*.

6   **(M)** Representative traces of light evoked inhibitory post-synaptic currents

7   (oIPSCs) in the SNr of D_1-Cre mice injected in the striatum with rAAV-DIO-

8   ChrmisonR as explained in **Figure 1L**. Note the presence of small oIPSCs

9   induced by blue light application using during calcium imaging.

1 **Figure S2 (related to main Figure 2). Functional localization of CB$_1$**

2 **receptors at mitochondrial membranes within the SNr.**

3 **(A)** Immunogold detection of CB$_1$ receptor by electron microscopy in WT and

4 *CB$_1$*-KO mice in SNr. White arrows, plasma membrane gold particles; pink

5 arrows, mitochondrial gold particles; scale bar: 500 nm.

6 **(B)** Schematic representation of the strategy employed for the generation of

7 DN22-*CB$_1$*-KI mouse line. LHA: left homology arm; RHA, right homology arm.

8 **(C)** Top left: qRT-PCR analysis of CB$_1$ mRNA in different brain regions from

9 WT, DN22-*CB$_1$*-KI and *CB$_1$*-KO mice. AMY, amygdala; HYP, hypothalamus;

10 STR, striatum; HPC, hippocampus; AON, anterior olfactory nucleus; PFC,

11 prefrontal cortex. n.d., not detected Top right and bottom: immunofluorescence

12 detection and representative images of CB$_1$ receptor in the brain of WT vs

13 DN22-*CB$_1$*-KI mice (*CB$_1$*-KO mice are shown as antibody negative control).

14 CA1, hippocampal region; SNr, substantia nigra pars reticulata; STR, striatum;

15 MC, motor cortex; AON, anterior olfactory nucleus; PFC, prefrontal cortex; CRB,

16 cerebellum.

17 **(D)** Immunogold detection of CB$_1$ receptor by electron microscopy in WT and

18 DN22-*CB$_1$*-KI mice in SNr. White arrows, plasma membrane gold particles; pink

19 arrows, mitochondrial gold particles; scale bar: 500 nm.

20 **(E)** Representative autoradiograms of brain sections from basal, 1 μM and 10

21 μM WIN-stimulated [^{35}S]GTPγS binding in WT mice.

22 **(F)** Relative quantification of WIN-mediated [^{35}S]GTPγS over basal level at 1μM

23 (left) and 10μM (right) doses in WT and DN22-*CB$_1$*-KI mice. SNr, substantia

24 nigra reticulata; STR, striatum; PFC, prefrontal cortex; OB, olfactory bulb; HYP,

hypothalamus; GPe, external globus pallidus; HPC, hippocampus; CB, cerebellum; BLA, basolateral amygdala; AON, anterior olfactory nucleus; NAC, nucleus accumbens.

(G) Representative autoradiograms of brain sections from WT, DN22-*CB₁*-KI and *CB₁*-KO mice incubated with [^{3H}] CP55.940.

(H) Relative quantification of bound [^{3H}] CP55.940 in WT, DN22-*CB₁*-KI and *CB₁*-KO slices. SNr, substantia nigra pars reticulata; STR, striatum; PFC, prefrontal cortex; OB, olfactory bulb; HYP, hypothalamus; GPe, external globus pallidus; HPC, hippocampus; CB, cerebellum; BLA, basolateral amygdala; AON, anterior olfactory nucleus; NAC, nucleus accumbens.

(I) Representative trace of mitochondrial respiration in a substantia nigra preparation from WT, DN22-*CB₁*-KI and *CB₁*-KO mice. Substrates are malate, pyruvate and glutamate. The inhibitory effect of WIN was observed when the respiration was coupled to ATP synthesis via the addition of Adenosine diphosphate (ADP, see **Table S1**).

Figure S3 (related to main Figure 3). MtCB$_1$ receptors and their signaling mediate the cataleptic effect of cannabinoids in the striatonigral circuits.

(A) Body weight (top panel) and muscular strength (measured by grid suspension test, bottom panel) of WT and DN22-*CB$_1$*-KI mice.

(B) Daily home cage locomotor activity of WT and DN22-*CB$_1$*-KI mice. Grey box indicate the night phase.

(C) Daily voluntary wheel running of WT and DN22-*CB$_1$*-KI mice. Grey box indicate the night phase.

(D) Time course plot showing eIPSCs amplitude before and after 3s depolarization (-70 to 0 mV grey line) in hippocampal slices obtained from WT and DN22-*CB$_1$*-KI mice.

(E) Representative traces of eIPSCs before and after 3s depolarization (-70 to 0 mV) in WT and DN22-*CB$_1$*-KI mice and averaged reduction of eIPSCs amplitude respect to baseline recorded during 3 sweeps after depolarization.

(F) Average paired pulse ratio (PPR) after optogenetic stimulation of striatonigral terminals in WT and DN22-*CB$_1$*-KI mice.

(G) Traces of GCaMP6 fluorescence variation (ΔF/F0) from sniffer cells in the absence (Vehicle) and in the presence of WIN when electrical stimulation (gray bars) of the striatonigral pathway in slices from DN22-*CB$_1$*-KI mice is applied. Plots are from the same cells in both conditions. Right: summary bar graphs comparing means ± SEM values of ΔF/F0 induced by electrical stimulation in all

sniffer cells responding and imaged over the SNr in Vehicle and WIN conditions in DN22-CB_1-KI mice.

(H) Effects of intra-SNr administration of the cell impermeable CB_1 antagonist Hemopressin (Hp, 22ng) on the antinociceptive effect of systemic THC (10mg/kg i.p.) in DN22-CB_1-KI mice.

(I) Effects of i.p. administration of the NK_1 receptor agonist GR73632 (75 μg/kg) on the antinociceptive effect of systemic THC (10mg/kg i.p.) respect to vehicle in DN22-CB_1-KI mice.

(J) Correlation between CB_1 fluorescence intensity in SNr (X axis) and immobility in the bar test induced by THC (Y axis) in D_1-CB_1-KO mice injected with rAAV-DIO-CB_1 (black dots) or with rAAV-DIO-DN22-CB_1 (grey dots) in the striatum.

(K) Effect of WIN (1µM) on mitochondrial respiration (oxygen consumption rate, OCR) in SN homogenates pre-treated with vehicle or GR736321 (1µM).

(L) Representative immunofluorescence of the mitochondrial protein TOMM20 and HA in Hela cells expressing pcDNA or mt-sAC. Scale bar: 10 µm.

(M) Representative pictures of HA-tag immunostaining in the dorsal striatum of D_1-Cre mice injected with control or Cre-dependent mt-sAC AAV. Scale bar 100µm.

(N) Western blotting for HA-tag, endogenous sAC, tubulin and Tomm20 after immuno-magnetic isolation of striatal mitochondria (Mito) compared to total cell

lysate (TCL) from D_1-Cre mice injected with control or Cre-dependent mt-sAC AAV in the dorsal striatum.

(O) Western blotting for HA-tag and endogenous sAC in SN homogenates (used for mitochondrial respiration, see **Figure 4I**) from D_1-Cre mice injected with control or Cre-dependent mt-sAC AAV in the dorsal striatum.

(P) Representative immunofluorescence and co-localization analysis of the mitochondrial protein TOMM20 and Myc in Hela cells expressing pcDNA, PKA-CA or MLS-PKA-CA. Scale bar: 10 µm. And Trypsin sensitivity assay (right).

(Q) Western blotting for Myc-tag, endogenous PKA, tubulin and Tomm20 after immuno-magnetic isolation of striatal mitochondria (Mito) compared to total cell lysate (TCL) from D_1-Cre mice injected with control or Cre-dependent PKA-CA or MLS-PKA-CA AAVs in the dorsal striatum.

(R) Western blotting for myc-tag in SN homogenates (used for mitochondrial respiration, see **Figure 4N**) from D_1-Cre mice injected with control or Cre-dependent PKA-CA or MLS-PKA-CA AAVs in the dorsal striatum.

1 **Figure S4. Proposed mechanisms for the subcellular specificity of**

2 **behavior control by CB$_1$ receptors in striatonigral circuits.**

3 At striatonigral terminals, activation of pmCB1 triggers inhibition of cytosolic

4 PKA, which in turn results in a reduction of Substance-P release and

5 subsequent decrease of pain perception. In the same terminals, activation of

6 mtCB$_1$ is responsible of motor impairment, by decreasing the release of GABA

7 on SNr neurons trough inhibition of mitochondrial activity.

8

1   **Table S1. Characterization of Mitochondrial respiration in SN extracts**

2   CI $_L$, ComplexI Leak; CI $_P$, ComplexI OXPHOS; CI & CII $_P$, ComplexI and

3   ComplexII OXPHOS; CII $_P$, ComplexII OXPHOS; ROX, Residual Oxigen

4   Consumption.

5   **Table S2. Statistical analysis. Related to Figure 1-4.**

6   **Table S3. Statistical analysis. Related to Figure S1-S3.**

7

REFERENCES

Bellocchio, L., Lafenetre, P., Cannich, A., Cota, D., Puente, N., Grandes, P., Chaouloff, F., Piazza, P., and Marsicano, G. (2010). Bimodal control of stimulated food intake by the endocannabinoid system. Nature Neuroscience 13, 281–283.

Bellocchio, L., Ruiz-Calvo, A., Chiarlone, A., Cabanas, M., Resel, E., Cazalets, J.R., Blazquez, C., Cho, Y.H., Galve-Roperh, I., and Guzman, M. (2016). Sustained Gq-Protein Signaling Disrupts Striatal Circuits via JNK. The Journal of neuroscience : the official journal of the Society for Neuroscience 36, 10611-10624.

Benard, G., Massa, F., Puente, N., Lourenco, J., Bellocchio, L., Soria-Gomez, E., Matias, I., Delamarre, A., Metna-Laurent, M., Cannich, A., *et al.* (2012). Mitochondrial CB(1) receptors regulate neuronal energy metabolism. Nature neuroscience 15, 558-564.

Boccella, S., Marabese, I., Guida, F., Luongo, L., Maione, S., and Palazzo, E. (2020). The Modulation of Pain by Metabotropic Glutamate Receptors 7 and 8 in the Dorsal Striatum. Curr Neuropharmacol 18, 34-50.

Borgelt, L.M., Franson, K.L., Nussbaum, A.M., and Wang, G.S. (2013). The pharmacologic and clinical effects of medical cannabis. Pharmacotherapy 33, 195-209.

Borgkvist, A., and Fisone, G. (2007). Psychoactive drugs and regulation of the cAMP/PKA/DARPP-32 cascade in striatal medium spiny neurons. Neuroscience and biobehavioral reviews 31, 79-88.

1 Borsook, D., Upadhyay, J., Chudler, E.H., and Becerra, L. (2010). A key role of
2 the basal ganglia in pain and analgesia--insights gained through human
3 functional imaging. Mol Pain 6, 27.

4 Bradford, M.M. (1976). A rapid and sensitive method for the quantitation of
5 microgram quantities of protein utilizing the principle of protein-dye binding.
6 Analytical Biochemistry 72, 248–254.

7 Brown, R.E. (2019). Review of Franz Joseph Gall: Naturalist of the mind,
8 visionary of the brain. Hist Psychol 22, 374-379.

9 Bucko, P.J., Lombard, C.K., Rathbun, L., Garcia, I., Bhat, A., Wordeman, L.,
10 Smith, F.D., Maly, D.J., Hehnly, H., and Scott, J.D. (2019). Subcellular drug
11 targeting illuminates local kinase action. Elife 8.

12 Busquets-Garcia, A., Bains, J., and Marsicano, G. (2018). CB1 Receptor
13 Signaling in the Brain: Extracting Specificity from Ubiquity.
14 Neuropsychopharmacology : official publication of the American College of
15 Neuropsychopharmacology 43, 4-20.

16 Chazalon, M., Paredes-Rodriguez, E., Morin, S., Martinez, A., Cristovao-
17 Ferreira, S., Vaz, S., Sebastiao, A., Panatier, A., Boue-Grabot, E., Miguelez, C.,
18 and Baufreton, J. (2018). GAT-3 Dysfunction Generates Tonic Inhibition in
19 External Globus Pallidus Neurons in Parkinsonian Rodents. Cell Rep 23, 1678-
20 1690.

21 Chen, W., Ennes, H.S., McRoberts, J.A., and Marvizon, J.C. (2018).
22 Mechanisms of mu-opioid receptor inhibition of NMDA receptor-induced
23 substance P release in the rat spinal cord. Neuropharmacology 128, 255-268.

1   Chomczynski, P., and Sacchi, N. (1987). Single-step method of RNA isolation

2   by acid guanidinium thiocyanate-phenol-chloroform extraction. Anal Biochem

3   162, 156-159.

4   Choo, Y.S. (2004). Mutant huntingtin directly increases susceptibility of

5   mitochondria to the calcium-induced permeability transition and cytochrome c

6   release. Human Molecular Genetics 13, 1407–1420.

7   Clapper, J.R., Moreno-Sanz, G., Russo, R., Guijarro, A., Vacondio, F., Duranti,

8   A., Tontini, A., Sanchini, S., Sciolino, N.R., Spradley, J.M., et al. (2010).

9   Anandamide suppresses pain initiation through a peripheral endocannabinoid

10 mechanism. Nat Neurosci 13, 1265–1270.

11 Cohen, K., Weizman, A., and Weinstein, A. (2019). Positive and Negative

12 Effects of Cannabis and Cannabinoids on Health. Clin Pharmacol Ther 105,

13 1139-1147.

14 Creighton, J. (2011). Targeting therapeutic effects: subcellular location matters.

15 Focus on "Pharmacological AMP-kinase activators have compartment-specific

16 effects on cell physiology". Am J Physiol Cell Physiol 301, C1293-1295.

17 Darmani,   N.A.,   and   Pandya,   D.K.   (2000).   Involvement   of   other

18 neurotransmitters in behaviors induced by the cannabinoid CB1 receptor

19 antagonist SR 141716A in naive mice. J Neural Transm (Vienna) 107, 931-945.

20 Deniau, J.M., Mailly, P., Maurice, N., and Charpier, S. (2007). The pars

21 reticulata of the substantia nigra: a window to basal ganglia output. Progress in

22 brain research 160, 151-172.

23 Donvito, G., Nass, S.R., Wilkerson, J.L., Curry, Z.A., Schurman, L.D., Kinsey,

24 S.G., and Lichtman, A.H. (2018). The Endogenous Cannabinoid System: A

25 Budding Source of Targets for Treating Inflammatory and Neuropathic Pain.

Neuropsychopharmacology : official publication of the American College of Neuropsychopharmacology 43, 52-79.

Dubreucq, S., Koehl, M., Abrous, D.N., Marsicano, G., and Chaouloff, F. (2010). CB1 receptor deficiency decreases wheel-running activity: consequences on emotional behaviours and hippocampal neurogenesis. Exp Neurol 224, 106-113.

Dwivedi, Y., and Pandey, G.N. (2008). Adenylyl cyclase-cyclicAMP signaling in mood disorders: role of the crucial phosphorylating enzyme protein kinase A. Neuropsychiatr Dis Treat 4, 161-176.

Eichel, K., and von Zastrow, M. (2018). Subcellular Organization of GPCR Signaling. Trends Pharmacol Sci 39, 200-208.

Fernandez-Ruiz, J., Moreno-Martet, M., Rodriguez-Cueto, C., Palomo-Garo, C., Gomez-Canas, M., Valdeolivas, S., Guaza, C., Romero, J., Guzman, M., Mechoulam, R., and Ramos, J.A. (2011). Prospects for cannabinoid therapies in basal ganglia disorders. Br J Pharmacol 163, 1365-1378.

Francisco, A., Engel, D.F., Figueira, T.R., Rogerio, F., de Bem, A.F., and Castilho, R.F. (2020). Mitochondrial NAD(P)(+) Transhydrogenase is Unevenly Distributed in Different Brain Regions, and its Loss Causes Depressive-like Behavior and Motor Dysfunction in Mice. Neuroscience 440, 210-229.

Freeze, B.S., Kravitz, A.V., Hammack, N., Berke, J.D., and Kreitzer, A.C. (2013). Control of basal ganglia output by direct and indirect pathway projection neurons. The Journal of neuroscience : the official journal of the Society for Neuroscience 33, 18531-18539.

Garcia, C., Palomo-Garo, C., Gomez-Galvez, Y., and Fernandez-Ruiz, J. (2016). Cannabinoid-dopamine interactions in the physiology and physiopathology of the basal ganglia. Br J Pharmacol 173, 2069-2079.

Garcia, G.C., Bartol, T.M., Phan, S., Bushong, E.A., Perkins, G., Sejnowski, T.J., Ellisman, M.H., and Skupin, A. (2019). Mitochondrial morphology provides a mechanism for energy buffering at synapses. Sci Rep 9, 18306.

Giuffrida, A., and Seillier, A. (2012). New insights on endocannabinoid transmission in psychomotor disorders. Prog Neuropsychopharmacol Biol Psychiatry 38, 51-58.

Griebel, G., Stemmelin, J., and Scatton, B. (2005). Effects of the cannabinoid CB1 receptor antagonist rimonabant in models of emotional reactivity in rodents. Biological Psychiatry 57, 261–267.

Guedouari, H., Daigle, T., Scorrano, L., and Hebert-Chatelain, E. (2017). Sirtuin 5 protects mitochondria from fragmentation and degradation during starvation. Biochimica et Biophysica Acta (BBA) - Molecular Cell Research 1864, 169–176.

Gutierrez-Rodriguez, A., Bonilla-Del Rio, I., Puente, N., Gomez-Urquijo, S.M., Fontaine, C.J., Egana-Huguet, J., Elezgarai, I., Ruehle, S., Lutz, B., Robin, L.M., *et al.* (2018). Localization of the cannabinoid type-1 receptor in subcellular astrocyte compartments of mutant mouse hippocampus. Glia 66, 1417-1431.

Häring, M., Kaiser, N., Monory, K., and Lutz, B. (2011). Circuit Specific Functions of Cannabinoid CB1 Receptor in the Balance of Investigatory Drive and Exploration. PLoS ONE 6, e26617.

Hebert-Chatelain, E., Desprez, T., Serrat, R., Bellocchio, L., Soria-Gomez, E., Busquets-Garcia, A., Pagano Zottola, A.C., Delamarre, A., Cannich, A., Vincent,

P., *et al.* (2016). A cannabinoid link between mitochondria and memory. Nature 539, 555-559.

Heimann, A.S., Gomes, I., Dale, C.S., Pagano, R.L., Gupta, A., de Souza, L.L., Luchessi, A.D., Castro, L.M., Giorgi, R., Rioli, V., *et al.* (2007). Hemopressin is an inverse agonist of CB1 cannabinoid receptors. Proceedings of the National Academy of Sciences of the United States of America 104, 20588-20593.

Ibsen, M.S., Connor, M., and Glass, M. (2017). Cannabinoid CB1 and CB2 Receptor Signaling and Bias. Cannabis Cannabinoid Res 2, 48-60.

Ilouz, R., Lev-Ram, V., Bushong, E.A., Stiles, T.L., Friedmann-Morvinski, D., Douglas, C., Goldberg, J.L., Ellisman, M.H., and Taylor, S.S. (2017). Isoform-specific subcellular localization and function of protein kinase A identified by mosaic imaging of mouse brain. Elife 6.

Jimenez-Blasco, D., Busquets-Garcia, A., Hebert-Chatelain, E., Serrat, R., Vicente-Gutierrez, C., Ioannidou, C., Gomez-Sotres, P., Lopez-Fabuel, I., Resch-Beusher, M., Resel, E., et al. (2020). Glucose metabolism links astroglial mitochondria to cannabinoid effects. Nature 583, 603-608.

Johnson, M.B., Young, A.D., and Marriott, I. (2016). The Therapeutic Potential of Targeting Substance P/NK-1R Interactions in Inflammatory CNS Disorders. Front Cell Neurosci 10, 296.

Kanellopoulos, A.K., Mariano, V., Spinazzi, M., Woo, Y.J., McLean, C., Pech, U., Li, K.W., Armstrong, J.D., Giangrande, A., Callaerts, P., *et al.* (2020). Aralar Sequesters GABA into Hyperactive Mitochondria, Causing Social Behavior Deficits. Cell 180, 1178-1197 e1120.

1 Kano, M., Ohno-Shosaku, T., Hashimotodani, Y., Uchigashima, M., and

2 Watanabe, M. (2009). Endocannabinoid-mediated control of synaptic

3 transmission. Physiol Rev 89, 309–380.

4 Klapoetke, N.C., Murata, Y., Kim, S.S., Pulver, S.R., Birdsey-Benson, A., Cho,

5 Y.K., Morimoto, T.K., Chuong, A.S., Carpenter, E.J., Tian, Z., et al. (2014).

6 Independent optical excitation of distinct neural populations. Nat Methods 11,

7 338–346.

8 Knight, R.T. (2007). Neuroscience. Neural networks debunk phrenology.

9 Science 316, 1578-1579.

10 Koch, M., Varela, L., Kim, J.G., Kim, J.D., Hernandez-Nuno, F., Simonds, S.E.,

11 Castorena, C.M., Vianna, C.R., Elmquist, J.K., Morozov, Y.M., et al. (2015).

12 Hypothalamic POMC neurons promote cannabinoid-induced feeding. Nature

13 519, 45–50.

14 Lahuna, O., and Jockers, R. (2018). [Mitochondrial signaling of G protein-

15 coupled receptors]. Biol Aujourdhui 212, 21-26.

16 Lemberger, T., Parlato, R., Dassesse, D., Westphal, M., Casanova, E., Turiault,

17 M., Tronche, F., Schiffmann, S.N., and Schutz, G. (2007). Expression of Cre

18 recombinase in dopaminoceptive neurons. BMC Neurosci 8, 4.

19 Lever, I.J., and Malcangio, M. (2002). CB(1) receptor antagonist SR141716A

20 increases capsaicin-evoked release of Substance P from the adult mouse

21 spinal cord. Br J Pharmacol 135, 21-24.

22 Livak, K.J., and Schmittgen, T.D. (2001). Analysis of relative gene expression

23 data using real-time quantitative PCR and the 2(-Delta Delta C(T)) Method.

24 Methods 25, 402-408.

Makrecka-Kuka, M., Krumschnabel, G., and Gnaiger, E. (2015). High-Resolution Respirometry for Simultaneous Measurement of Oxygen and Hydrogen Peroxide Fluxes in Permeabilized Cells, Tissue Homogenate and Isolated Mitochondria. Biomolecules 5, 1319-1338.

Marsicano, G., Goodenough, S., Monory, K., Hermann, H., Eder, M., Cannich, A., Azad, S.C., Cascio, M.G., Gutierrez, S.O., van der Stelt, M.*, et al.* (2003). CB1 cannabinoid receptors and on-demand defense against excitotoxicity. Science 302, 84-88.

Marsicano, G., and Kuner, R. (2008). Anatomical distribution of receptors, ligands and enzymes in the brain and the spinal cord: circuitries and neurochemistry. In Cannabinoids and the brain, A. Kofalvi, ed. (New York: Springer), pp. 161-202.

Martin, J.L., Gadegbeku, B., Wu, D., Viallon, V., and Laumon, B. (2017). Cannabis, alcohol and fatal road accidents. PloS one 12, e0187320.

Martinez, A., Macheda, T., Morgese, M.G., Trabace, L., and Giuffrida, A. (2012). The cannabinoid agonist WIN55212-2 decreases L-DOPA-induced PKA activation and dyskinetic behavior in 6-OHDA-treated rats. Neurosci Res 72, 236-242.

Metna-Laurent, M., Mondesir, M., Grel, A., Vallee, M., and Piazza, P.V. (2017). Cannabinoid-Induced Tetrad in Mice. Curr Protoc Neurosci 80, 9 59 51-59 59 10.

Monory, K., Blaudzun, H., Massa, F., Kaiser, N., Lemberger, T., Schutz, G., Wotjak, C.T., Lutz, B., and Marsicano, G. (2007). Genetic dissection of behavioural and autonomic effects of Delta(9)-tetrahydrocannabinol in mice. PLoS biology 5, e269.

Nadal, X., La Porta, C., Andreea Bura, S., and Maldonado, R. (2013). Involvement of the opioid and cannabinoid systems in pain control: New insights from knockout studies. European Journal of Pharmacology 716, 142–157.

Niswender, C.M., Willis, B.S., Wallen, A., Sweet, I.R., Jetton, T.L., Thompson, B.R., Wu, C., Lange, A.J., and McKnight, G.S. (2005). Cre recombinase-dependent expression of a constitutively active mutant allele of the catalytic subunit of protein kinase A. Genesis 43, 109-119.

Oliveira da Cruz, J., Busquets-Garcia, A., Zhao, Z., Varilh, M., Lavanco, G., Bellocchio, L., Robin, L., Cannich, A., Julio-Kalajzić, F., Lesté-Laserre,T., Maitre, M., Drago, F., Marsicano, G., Soria-Gomez, E. (2020). Specific Hippocampal Interneurons Shape Consolidation of Recognition Memory. Cell Reports. 32(7): 108046. doi: 10.1016/j.celrep.2020.108046

Oshita, K., Inoue, A., Tang, H.B., Nakata, Y., Kawamoto, M., and Yuge, O. (2005). CB(1) cannabinoid receptor stimulation modulates transient receptor potential vanilloid receptor 1 activities in calcium influx and substance P Release in cultured rat dorsal root ganglion cells. J Pharmacol Sci 97, 377-385.

Pagano Zottola , A.C., Soria-Gomez, E., Bonilla-del-Río, I., Muguruza, C., Terral, G., Robin, L.M., Oliveira da Cruz, J.F., Redon, B., Lesté-Lasserre, T., Tolentino-Cortes, T Puente, N., Barreda-Gómez, G Chaouloff, F., Callado, L.F., Grandes, P., Marsicano, G., Bellocchio, L. (2020). A new mutant mouse model lacking mitochondrial-associated CB1 receptor. Biorxiv.

Pautrat, A., Rolland, M., Barthelemy, M., Baunez, C., Sinniger, V., Piallat, B., Savasta, M., Overton, P.G., David, O., and Coizet, V. (2018). Revealing a novel

nociceptive network that links the subthalamic nucleus to pain processing. ELife 7, e36607.

Paxinos, G., and Franklin, K.B.J. (2001). The Mouse Brain in Stereotaxic Coordinates (S. Diego (USA): Academic Press).

Pertwee, R.G. (2001). Cannabinoid receptors and pain. Progress in neurobiology 63, 569-611.

Prashad, S., and Filbey, F.M. (2017). Cognitive motor deficits in cannabis users. Curr Opin Behav Sci 13, 1-7.

Puente, N., Bonilla-Del Río, I., Achicallende, S., Nahirney, P.C., and Grandes, P. (2019). High-resolution Immunoelectron Microscopy Techniques for Revealing Distinct Subcellular Type 1 Cannabinoid Receptor Domains in Brain. Bioprotocol 9.

Qi, G., Mi, Y., and Yin, F. (2019). Cellular Specificity and Inter-cellular Coordination in the Brain Bioenergetic System: Implications for Aging and Neurodegeneration. Front Physiol 10, 1531.

Rajendran, L., Knolker, H.J., and Simons, K. (2010). Subcellular targeting strategies for drug design and delivery. Nat Rev Drug Discov 9, 29-42.

Rangaraju, V., Calloway, N., and Ryan, T.A. (2014). Activity-driven local ATP synthesis is required for synaptic function. Cell 156, 825-835.

Ray, A.P., Chebolu, S., Ramirez, J., and Darmani, N.A. (2009). Ablation of least shrew central neurokinin NK1 receptors reduces GR73632-induced vomiting. Behavioral neuroscience 123, 701-706.

Redon, B., Violleau, C., Georges, F., Marsicano, G., and Chaouloff, F. (2020). The ergogenic impact of the glucocorticoid prednisolone does not translate into increased running motivation in mice. Psychoneuroendocrinology 111, 104489.

1 Rozenfeld, R., and Devi, L.A. (2008). Regulation of CB1 cannabinoid receptor

2 trafficking by the adaptor protein AP-3. FASEB journal : official publication of the

3 Federation of American Societies for Experimental Biology 22, 2311-2322.

4 Ruehle, S., Remmers, F., Romo-Parra, H., Massa, F., Wickert, M., Wortge, S.,

5 Haring, M., Kaiser, N., Marsicano, G., Pape, H.C., and Lutz, B. (2013).

6 Cannabinoid CB1 Receptor in Dorsal Telencephalic Glutamatergic Neurons:

7 Distinctive Sufficiency for Hippocampus-Dependent and Amygdala-Dependent

8 Synaptic and Behavioral Functions. The Journal of neuroscience : the official

9 journal of the Society for Neuroscience 33, 10264-10277.

10 Sales-Carbonell, C., Rueda-Orozco, P.E., Soria-Gomez, E., Buzsaki, G.,

11 Marsicano, G., and Robbe, D. (2013). Striatal GABAergic and cortical

12 glutamatergic neurons mediate contrasting effects of cannabinoids on cortical

13 network synchrony. Proceedings of the National Academy of Sciences of the

14 United States of America 110, 719-724.

15 Simpson, D. (2005). Phrenology and the neurosciences: contributions of F. J.

16 Gall and J. G. Spurzheim. ANZ J Surg 75, 475-482.

17 Skalhegg, B.S., and Tasken, K. (2000). Specificity in the cAMP/PKA signaling

18 pathway. Differential expression,regulation, and subcellular localization of

19 subunits of PKA. Front Biosci 5, D678-693.

20 Soria-Gomez, E., Bellocchio, L., Reguero, L., Lepousez, G., Martin, C.,

21 Bendahmane, M., Ruehle, S., Remmers, F., Desprez, T., Matias, I., *et al.*

22 (2014). The endocannabinoid system controls food intake via olfactory

23 processes. Nature neuroscience 17, 407-415.

24 Steiner, H., Bonner, T.I., Zimmer, A.M., Kitai, S.T., and Zimmer, A. (1999).

25 Altered gene expression in striatal projection neurons in CB1 cannabinoid

receptor knockout mice. Proceedings of the National Academy of Sciences of the United States of America 96, 5786-5790.

Steinhoff, M.S., von Mentzer, B., Geppetti, P., Pothoulakis, C., and Bunnett, N.W. (2014). Tachykinins and their receptors: contributions to physiological control and the mechanisms of disease. Physiol Rev 94, 265-301.

Szabo, B., Wallmichrath, I., Mathonia, P., and Pfreundtner, C. (2000). Cannabinoids inhibit excitatory neurotransmission in the substantia nigra pars reticulata. Neuroscience 97, 89-97.

Taylor, A.M., Becker, S., Schweinhardt, P., and Cahill, C. (2016). Mesolimbic dopamine signaling in acute and chronic pain: implications for motivation, analgesia, and addiction. Pain 157, 1194-1198.

Terral, G., Busquets-Garcia, A., Varilh, M., Achicallende, S., Cannich, A., Bellocchio, L., Bonilla-Del Río, I., Massa, F., Puente, N., Soria-Gomez, E., et al. (2019). CB1 Receptors in the Anterior Piriform Cortex Control Odor Preference Memory. Current Biology 29, 2455-2464.e5.

Vallee, M., Vitiello, S., Bellocchio, L., Hebert-Chatelain, E., Monlezun, S., Martin-Garcia, E., Kasanetz, F., Baillie, G.L., Panin, F., Cathala, A., et al. (2014). Pregnenolone can protect the brain from cannabis intoxication. Science 343, 94-98.
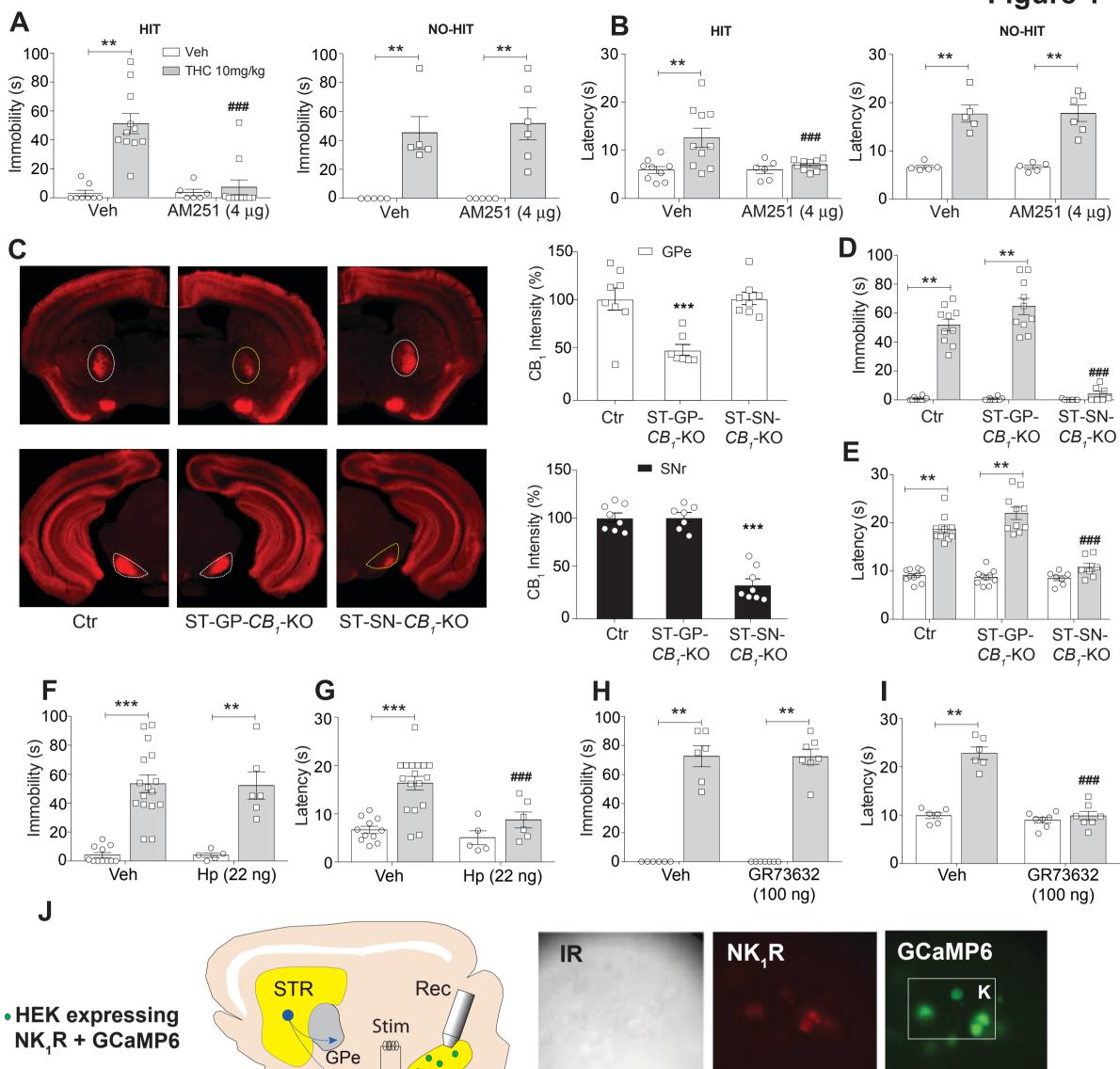
Valsecchi, F., Konrad, C., and Manfredi, G. (2014). Role of soluble adenylyl cyclase in mitochondria. Biochim Biophys Acta 1842, 2555-2560.

Vos, M., Lauwers, E., and Verstreken, P. (2010). Synaptic mitochondria in synaptic transmission and organization of vesicle pools in health and disease. Front Synaptic Neurosci 2, 139.
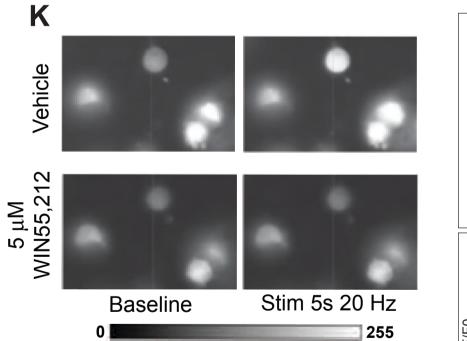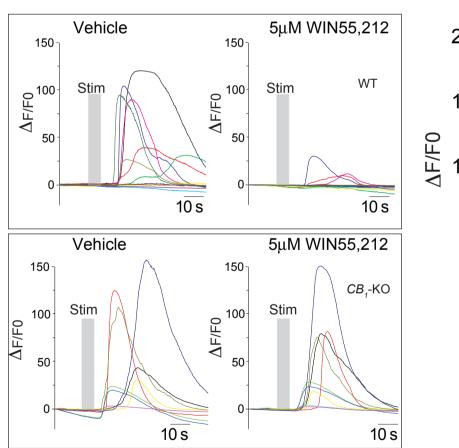
1 Wilson, R.I., Kunos, G., and Nicoll, R.A. (2001). Presynaptic specificity of

2 endocannabinoid signaling in the hippocampus. Neuron 31, 453-462.

3 Woodhams, S.G., Chapman, V., Finn, D.P., Hohmann, A.G., and Neugebauer,

4 V. (2017). The cannabinoid system and pain. Neuropharmacology 124, 105-

5 120.

6 Zaelzer, C., Gizowski, C., Salmon, C.K., Murai, K.K., and Bourque, C.W.

7 (2018). Detection of activity-dependent vasopressin release from neuronal

8 dendrites and axon terminals using sniffer cells. J Neurophysiol 120, 1386-

9 1396.

10 Zhao, Z., Soria-Gomez, E., Varilh, M., Covelo, A., Julio-Kalajzic, F., Cannich,

11 A., Castiglione, A., Vanhoutte, L., Duveau, A., Zizzari, P Beyeler, A., Cota, D.,

12 Bellocchio, L., Busquets-Garcia, A., Marsicano, G. (2020). A novel cortical

13 mechanism for top-down control of water intake. Curr Biol 30, 4789-4798.

14 Zhou, F.M. (2016). The Substantia Nigra Pars Reticulata. In Handbook of

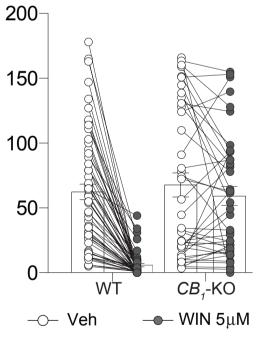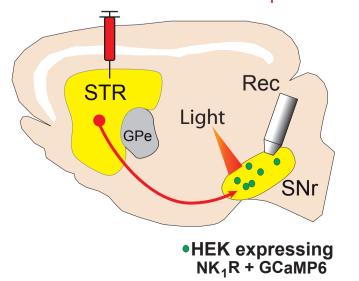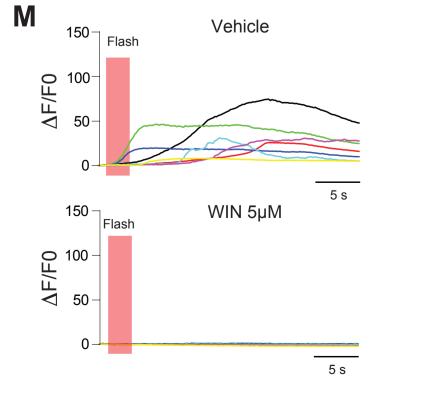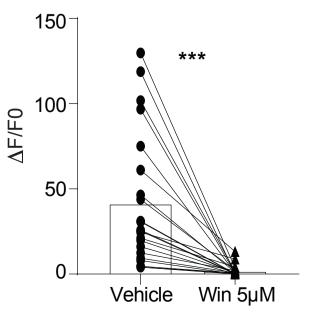15 Behavioral Neuroscience, (Elsevier), pp. 293–316.

16

Figure 1

Figure 2

Figure 3

Figure 4

A

HIT   NO-HIT

SNr   SNr

-2.92 mm

-3.28 mm

-3.88 mm

B

□ Veh ■ THC 10mg/kg

HIT

**

###

Locomotor activity (A.U.)

Veh   AM251 (4 µg)

NO-HIT

**   **

Locomotor activity (A.U.)

Veh   AM251 (4 µg)

C

AAV-FRT-iCre-EGFP   AAV-retro-BLFP

Ctr

STR   SNr or GPe

AAV-FRT-iCre-EGFP   AAV-retro-FLP-BLFP

FLP

STR   SNr or GPe

GPe-FLP   ST-GP-CB₁-KO

STR   GPe

SNr-FLP   ST-SN-CB₁-KO

STR   SNR

D

Ctr   ST-GP-CB₁-KO   ST-SN-CB₁-KO

CB₁ / D₁

ec   ec

CB₁ / D₂

ec

% of CB₁/D₁+ cells

**   ns

Ctr   ST-GP-CB₁-KO   ST-SN-CB₁-KO

% of CB₁/D₂+ cells

**   ns

Ctr   ST-GP-CB₁-KO   ST-SN-CB₁-KO

E

□ Veh ■ THC 10mg/kg

***   ***   ***

Locomotor activity (A.U.)

Ctr   ST-GP-CB₁-KO   ST-SN-CB₁-KO

F

□ Veh ■ THC 10mg/kg

**   **

Immobility (s)

Veh   GR73632 75 µg/kg

G

□ Veh ■ THC 10mg/kg

**   ###

Latency (s)

Veh   GR73632 (75 µg/kg)

H

SP "Sniffer Cell" System

NK₁ Receptor

↓IP3
↑Ca²⁺   GCaMP
"Dim"

+SP

↑IP3
↑Ca²⁺   GCaMP
"Bright"

NK₁R-mCherry   GCaMP6s   Merge

a   b

Fluorescence (A.U.)

*   *   *

a   b

GCaMP6s Time=0s

GCaMP6s Time=180s

Substance P (10nM)

Fluor. Intensity (A.U.)

Time (s)

EC₅₀= 5.088nM

ΔF/F₀

[SP] (M)

I

Substance-P 100pM   Substance-P 1nM   Substance-P 10nM   Substance-P 100nM

Ca²⁺ (F₄₈₈ normalized)

5 min

● Ctr / GCaMP6s   ● NK₁-mCherry / GCaMP6s

J

Veh   GCaMP6s

ΔF / F0

Stim

10s

K

Veh   GCaMP6s NK1R-mCherry

ΔF / F0

Stim

10s

CP122721   GCaMP6s NK1R-mCherry

ΔF / F0

Stim

10s

L

***

ΔF

Vehicle GCaMP6s   Vehicle GCaMP6s NK1R-mCherry   CP122721

M

ΔF

Control   Vehicle   WIN

N

WIN   WIN

Substance-P 1nM   Substance-P 10nM

Ca²⁺ (F₄₈₈ normalized)

5 min

O

λ=660nm

500 pA

50 ms

λ=460nm

500 pA

50 ms

Figure S2

Subcellular Specificity of Behavioral Control